Distinct purinergic signaling pathways in prepubescent mouse spermatogonia

David Fleck,[1] Nadine Mundt,[1] Felicitas Bruentgens,[1] Petra Geilenkirchen,[2] Patricia A. Machado,[1] Thomas Veitinger,[1] Sophie Veitinger,[1] Susanne M. Lipartowski,[1] Corinna H. Engelhardt,[1] Marco Oldiges,[2] Jennifer Spehr,[1] and Marc Spehr[1]

[1]Department of Chemosensation, Institute for Biology II, RWTH Aachen University, D-52074 Aachen, Germany
[2]Institute of Bio- and Geosciences (IBG), IBG-1: Biotechnology, Research Center Jülich, D-52425 Jülich, Germany

Spermatogenesis ranks among the most complex, yet least understood, developmental processes. The physiological principles that control male germ cell development in mammals are notoriously difficult to unravel, given the intricate anatomy and complex endo- and paracrinology of the testis. Accordingly, we lack a conceptual understanding of the basic signaling mechanisms within the testis, which control the seminiferous epithelial cycle and thus govern spermatogenesis. Here, we address paracrine signal transduction in undifferentiated male germ cells from an electrophysiological perspective. We identify distinct purinergic signaling pathways in prepubescent mouse spermatogonia, both in vitro and in situ. ATP—a dynamic, widespread, and evolutionary conserved mediator of cell to cell communication in various developmental contexts—activates at least two different spermatogonial purinoceptor isoforms. Both receptors operate within nonoverlapping stimulus concentration ranges, display distinct response kinetics and, in the juvenile seminiferous cord, are uniquely expressed in spermatogonia. We further find that spermatogonia express Ca^{2+}-activated large-conductance K^+ channels that appear to function as a safeguard against prolonged ATP-dependent depolarization. Quantitative purine measurements additionally suggest testicular ATP-induced ATP release, a mechanism that could increase the paracrine radius of initially localized signaling events. Moreover, we establish a novel seminiferous tubule slice preparation that allows targeted electrophysiological recordings from identified testicular cell types in an intact epithelial environment. This unique approach not only confirms our in vitro findings, but also supports the notion of purinergic signaling during the early stages of spermatogenesis.

The Journal of General Physiology

INTRODUCTION

Spermatogenesis ranks among the most complex, yet least understood, developmental processes in postnatal life. Initiated 5–7 d postpartum in rodents (Kolasa et al., 2012), this intricate course of mass cell proliferation and transformation events generates fertile haploid spermatozoa from diploid spermatogonial stem cells (SSCs). The seminiferous tubule represents the functional unit of the testis. Along its epithelium, spermatogenesis has been simplified morphologically by attribution of sequential cellular stages, which progress through coordinated and precisely timed cycles (Hess and de Franca, 2008). However, prepubescent immature seminiferous tubules/cords are exclusively built by three cell types, i.e., Sertoli cells, peritubular cells, and spermatogonia (Bellvé et al., 1977). Although difficult to discriminate both morphologically and molecularly (Jan et al., 2012), premeiotic germ cells of the spermatogonial lineage comprise a heterogeneous population (Chiarini-Garcia and Russell, 2002), including SSCs, proliferating A_{paired} and $A_{aligned}$ cells, and differentiating A1-A4, intermediate and B spermatogonia (Kolasa et al., 2012). Both Sertoli and germ cells have developed elaborate, yet ill-defined mechanisms of functional communication (Cheng and Mruk, 2002). Multidirectional interactions among germ cells as well as between germ and somatic cells balance SSC self-renewal and differentiation, synchronize stage transitions, regulate blood–testis barrier dynamics, and control epithelial cyclicity via autocrine, paracrine, and endocrine feedback (Heindel and Treinen, 1989). Precisely regulated cellular communication within the seminiferous epithelium is thus imperative for spermatogenesis and reproduction.

In numerous developmental processes, purinergic signaling is emerging as a critical component of paracrine communication networks (Abbracchio et al., 2009; Praetorius and Leipziger, 2009). As a widespread and evolutionary conserved route for cell to cell interactions, extracellular ATP targets members of the P2 purinoceptor family (Burnstock, 1990). P2 receptors divide into two distinct classes: metabotropic P2Y (Barnard et al., 1994) and ionotropic P2X receptors (Bean

Correspondence to Marc Spehr: m.spehr@sensorik.rwth-aachen.de

Abbreviations used: BzATP, 2′(3′)-*O*-(4-Benzoylbenzoyl) ATP; DIV, day in vitro; FSH, follicle-stimulating hormone; IR-DIC, infrared-optimized differential interference contrast; ISI, interstimulus interval; RT, room temperature; siRNA, small interfering RNA; SSC, spermatogonial stem cell.

The Rockefeller University Press $30.00
J. Gen. Physiol. 2016 Vol. 148 No. 3 253–271
www.jgp.org/cgi/doi/10.1085/jgp.201611636

and Friel, 1990; Bean, 1992), comprising eight (P2Y) or seven (P2X) isoforms, respectively (Alexander et al., 2011). The complexity of both receptor families and the broad spatiotemporal response scales of P2 receptors confer functional specificity and flexibility to a ubiquitous signaling pathway (Jarvis and Khakh, 2009). P2X receptors form homo- or heterotrimers that function as ligand-gated cation channels. So far, six homomeric and several heteromeric channels have been described, each exhibiting distinct ATP affinities, pharmacological profiles, and desensitization kinetics (Khakh and North, 2012). Notably, all P2X receptors display substantial Ca^{2+} permeability and thus represent major components of the cellular Ca^{2+} signaling "toolkit" (Clapham, 2007). This role as a Ca^{2+} gate underlies the long-term developmental effects of purinergic signaling on cell proliferation, differentiation, migration, and turnover (Burnstock, 2008).

Recently, we and others suggested that purinergic signaling constitutes a critical component of testicular auto/paracrine communication (Filippini et al., 1994; Foresta et al., 1995; Gelain et al., 2003; Ko et al., 2003; Poletto Chaves et al., 2006; Antonio et al., 2009; Veitinger et al., 2011). In Sertoli cells, P2X2- and P2Y2-dependent Ca^{2+} signals counteract various effects mediated by follicle-stimulating hormone (FSH) and alter estradiol production, enzyme activity, and secretory behavior (Rudge et al., 1995; Meroni et al., 1998; Rossato et al., 2001; Gelain et al., 2005; Veitinger et al., 2011). Moreover, ATP secretion from Sertoli cells is itself under endocrine control (Lalevée et al., 1999; Gelain et al., 2005). However, whether spermatogonia are also targets of paracrine purinergic signaling and, if so, which molecular machinery mediates ATP sensitivity in premeiotic germ cells is currently unclear.

Here, we used gene expression analysis, immuno- and bioanalytical chemistry, protein knockdown, and single cell electrophysiology to investigate purinoceptor signaling mechanisms in spermatogonia from prepubescent mice both in vitro and in situ. We identify a multidimensional ATP response pathway that consists of both P2X4 and P2X7 receptor isoforms as well as Ca^{2+}-activated large conductance (BK) K^+ channels. This channel profile endows spermatogonia with distinct and dynamic response features over a broad range of stimulus concentrations. Cooperatively activated by depolarization and increased cytoplasmic Ca^{2+} (Fakler and Adelman, 2008), BK channels, in turn, provide a negative feedback mechanism that counteracts the electrophysiological effects of P2X receptor activation. In addition, P2X signaling itself acts as a regulator of testicular ATP release, providing a parallel positive feedback pathway. Consistency of results from primary cell culture and an intact acute seminiferous tubule slice preparation substantiates the physiological relevance of our findings.

MATERIALS AND METHODS

Animals

All animal procedures were approved by local authorities and in compliance with European Union legislation (Directive 86/609/EEC) and recommendations by the Federation of European Laboratory Animal Science Associations (FELASA). C57BL/6 mice (Charles River) were housed in groups of both sexes (room temperature [RT]; 12:12 h light–dark cycle; food and water available ad libitum). If not stated otherwise, experiments used 7-d-old males.

Chemicals and solutions

The following solutions were used: (S_1) HEPES-buffered extracellular solution containing (mM) 145 NaCl, 5 KCl, 1 $CaCl_2$, 0.5 $MgCl_2$, and 10 HEPES; pH = 7.3 (adjusted with NaOH); osmolarity = 300 mOsm (adjusted with glucose). (S_2) Oxygenated (95% O_2, 5% CO_2) extracellular solution containing (mM) 120 NaCl, 25 $NaHCO_3$, 5 KCl, 0.5 $MgCl_2$, 1.0 $CaCl_2$, 5 *N*,*N*-bis(2-hydroxyethyl)-2-aminoethanesulfonic acid (BES), and 10 glucose; pH = 7.3 (NaOH); 300 mOsm (glucose). (S_3) Extracellular low Ca^{2+} solution containing (mM) 145 NaCl, 5 KCl, 2.5 $CaCl_2$, 0.5 $MgCl_2$, 10 HEPES, and 5 EGTA; pH = 7.3 (NaOH); osmolarity = 300 mOsm (glucose), $[Ca^{2+}]_{free}$ = ~110 nM. (S_4) Extracellular TEA solution containing (mM) 120 NaCl, 15 TEACl, 5 KCl, 1 $CaCl_2$, 0.5 $MgCl_2$, and 10 HEPES; pH = 7.3 (NaOH); osmolarity = 300 mOsm (glucose). (S_5) Standard pipette solution containing (mM) 143 KCl, 2 KOH, 1 EGTA, 0.3 $CaCl_2$, 10 HEPES, and 1 Na-GTP ($[Ca^{2+}]_{free}$ = 110 nM); pH = 7.1 (adjusted with KOH); osmolarity = 290 mOsm (glucose). (S_6) Cs^+-based pipette solution containing (mM) 143 CsCl, 2 CsOH, 1 EGTA, 0.3 $CaCl_2$, 10 HEPES, and 1 Na-GTP ($[Ca^{2+}]_{free}$ = 110 nM); pH = 7.1 (adjusted with CsOH); osmolarity = 290 mOsm (glucose). (S_7) Standard blocking solution containing 5% (anti-P2X4, anti-P2X7, anti-Sloα1) or 10% (anti-DAZL) normal goat serum (Thermo Fisher Scientific), 10 mg/ml BSA, 0.3% Triton X-100, and 0.02% NaN_3 in $PBS^{-/-}$ (100 mM). (S_8) Cell culture blocking solution containing 1% BSA and 0.1% Triton X-100 in $PBS^{-/-}$ (100 mM). (S_9) Standard washing solution containing 10 mg/ml BSA in $PBS^{-/-}$ (100 mM). (S_{10}) Standard staining solution containing 3% BSA (IgG free, protease free), 0.05% NaN_3, and Alexa Fluor 488 or 633 streptavidin conjugate (1:800; Thermo Fisher Scientific) in $PBS^{-/-}$ (100 mM). (S_{11}) Standard co-culture medium (adopted and modified from Iwanami et al. [2006]) consisting of DMEM (low glucose, pyruvate; Thermo Fisher Scientific) complemented with 10 ng/ml epidermal growth factor, 10% fetal calf serum (Thermo Fisher Scientific), 1 ng/ml FSH, 0.2 ng/ml growth hormone releasing factor, 5 µg/ml insulin, 10 ng/ml insulin-like growth factor, 1% MEM nonessential amino acid solution (Thermo Fisher Scientific), 0.01%

Table 1. **Specific primer pairs used for PCR amplification**

Target	Forward primer 5′-3′	Reverse primer 5′-3′	Size
			bp
P2X1	GAGAGTCGGGCCAGGACTTC	GCGAATCCCAAACACCTTGA	233
P2X2	TCCCTCCCCCACCTAGTCAC	CACCACCTGCTCAGTCAGAGC	149
P2X3	CTGCCTAACCTCACCGACAAG	AATACCCAGAACGCCACCC	150
P2X4	CCCTTTGCCTGCCCAGATAT	CCGTACGCCTTGGTGAGTGT	145
P2X5	GGAAGATAATGTTGAGGTTGA	TCCTGACGAACCCTCTCCAGT	81
P2X5b	GCTGCCTCCCACTGCAACCC	AAGCCCCAGCACCCATGAGC	253
P2X6	TCCAGAGCATCCTTCCGTTCC	GGCACCAGCTCCAGATCTCA	152
P2X7	GCACGAATTATGGCACCGTC	CCCCACCCTCTGTGACATTCT	171
$P2X2_{splice}$	GACCTCCATCGGGGTGGGCT	ATGTCCTGGGAGCCGAAGCG	116
$P2X7_{splice}$	GTCTCGCCTACCGGAGCAACG	TGGGGTCCGTGGATGTGGAGT	237
β-actin	GTCTTCCCCTCCATCGTGG	TGGATGCCACAGGATTCC	750

nucleoside solution, 100 U/ml penicillin, 100 µg/ml streptomycin, 5 µM retinol acetate, 0.5 mM sodium pyruvate, 100 nM testosterone, and 5 µg/ml transferrin.

Free Ca^{2+} concentrations were calculated using WEBMAXC Extended. If not stated otherwise, chemicals were purchased from Sigma-Aldrich. Alexa Fluor hydrazide was purchased from Thermo Fisher Scientific; 3-[[5-(2,3-Dichlorophenyl)-1H-tetrazol-1-yl] methyl]pyridine hydrochloride (A-438079), Adenosine 5′-(α,β-methylene)diphosphate sodium salt (AOPCP), and 1-Amino-4-(4-chlorophenyl)aminoanthraquinone-2-sulfonic acid sodium salt (PSB 069) were purchased from Tocris Bioscience; and iberiotoxin was purchased from Abcam. PSB-POM144 (Lee et al., 2015) was provided by C.E. Müller (University of Bonn, Bonn, Germany). Final solvent concentrations were ≤0.1%. When high ATP concentrations (≥1 mM) were used, pH was readjusted. Solutions and pharmacological agents were applied either by the bath or from air pressure–driven reservoirs via an 8-in-1 multi-barrel "perfusion pencil" (Science Products). Changes in focal superfusion (Veitinger et al., 2011) were software controlled and, if required, synchronized with data acquisition by TTL input to 12V DC solenoid valves using a TIB 14S digital output trigger interface (HEKA).

Slice preparation

Male mice were sacrificed on postnatal day 7 (P7) by decapitation with sharp surgical scissors. Testes were rapidly dissected, each tunica albuginea was removed, and seminiferous tubules were embedded in 4% low-gelling temperature agarose (VWR) and placed in oxygenated S_2. 200-µm slices were cut with a VT1000S vibratome (speed: 0.15 mm/s; frequency: 65 Hz; amplitude: 1 mm; Leica Biosystems) and transferred to a submerged, oxygenated storage container (S_2; RT) until use.

Cell culture

After dissection of both testes on P7 and removal of the tunica albuginea, the seminiferous tubules from juvenile/prepubescent mice were placed in MEM (Thermo Fisher Scientific) containing 1 mg/ml collagenase (8 min; 37°C). Digestion was stopped by the addition of serum-containing DMEM (Thermo Fisher Scientific). The suspension was centrifuged (8 min; 400 *g*) and the supernatant discarded. The pellet was resuspended in 0.05% Trypsin-EDTA (Thermo Fisher Scientific), incubated (5 min, 37°C), and centrifuged (10 min; 400 *g*). After discarding the supernatant, the pellet was resuspended in culture medium (S_{11}). Cells were plated on glass coverslips in 35-mm dishes at densities of ∼2.5 × 10^5 cells per dish and placed in a humidified incubator for 3 d (37°C; 5% CO_2). On the fourth day in vitro (DIV4), incubation temperature was reduced (34°C; 5% CO_2). After addition of 1 ml S_{11} on DIV1, one-third of the medium was replaced every day. Experiments were performed from DIV4 to DIV7.

Gene expression analysis

Total RNA from cultured spermatogonia, testis, brain, and spinal cord was isolated using the RNeasy Mini kit (QIAGEN) according to the manufacturer's instructions. cDNA was transcribed using RevertAid H Minus M-MuLV reverse transcription (Fermentas) according to the manufacturer's instructions. Controls in which the reverse transcription step was omitted were routinely performed. PCR amplification was performed during 30 thermal cycles (94°C, 20 s; 52–63°C, 20 s; 72°C, 20 s). To confirm the anticipated size of the product, PCR products were visualized on an agarose gel via GelRed (VWR) staining. The specific primer pairs used for PCR amplification are listed in Table 1.

For qPCR, we used the QuantiFast SYBR Green PCR kit (QIAGEN) and an iQ5 thermal cycler (Bio-Rad Laboratories) according to the manufacturer's instructions. α1A-tubulin was used to normalize the amount of target mRNA in the different cDNA populations tested. Relative mRNA levels were then calculated using the threshold cycle (Ct) value and the comparative Ct method. The primer pairs used for qPCR are listed in Table 2.

Table 2. **Primer pairs used for qPCR**

Target	Forward primer 5′-3′	Reverse primer 5′-3′	Size
			bp
P2X4	TCCTGGCTTACGTCATTGGG	AGAAGTGTTGGTCACAGCCA	116
P2X7	CCCAGATGGACTTCTCCGAC	GGACTTAGGGGCCACCTCTT	116
α1A-tubulin	TCCCAAAGATGTCAATGCTG	CACAGTGGGAGGCTGGTAAT	115

Protein knockdown

For small interfering RNA (siRNA) experiments, either Sertoli cells or spermatogonia were transfected 12–24 h before experiments using Lipofectamine 2000 (Thermo Fisher Scientific) according to the manufacturer's instructions. Before transfection, the culture medium was replaced with antibiotic-free medium. siRNA (Applied Biosystems/Ambion) was cotransfected with BLOCK-iT fluorescent oligo (FITC labeled; Thermo Fisher Scientific). Opti-MEM I Reduced Serum Medium (500 µl; Thermo Fisher Scientific) containing 6 µl Lipofectamine 2000, 502.5 ng siRNA (75 nM), and 1.875 µl BLOCK-iT fluorescent oligo (75 nM) was added to each culture dish. Transfected cells were identified by FITC fluorescence. We used the following Silencer Select Pre-designed siRNA constructs to down-regulate receptor protein expression: P2X4 RNAi1, #s71184; P2X4 RNAi2, #s71185; P2X2 RNAi1, #s106892; P2X2 RNAi2, #s106893; and P2X7 RNAi, #s71189. As negative control, we used Silencer Select negative control #1 and #2 siRNA.

LC-MS/MS analysis

Seminiferous tissue samples were dissected as described above (Slice preparation). Individual sample weight was recorded for post hoc normalization. Samples and controls were exposed to either a defined concentration of ATP (10 µM), 2′(3′)-*O*-(4-Benzoylbenzoyl) ATP (BzATP; 300 µM), or volume-matched physiological saline (S_1) for 5 min. Next, samples were centrifuged (3 min; 4,000 *g*; 4°C) and filtered (10 min; 17,000 *g*; 4°C). All protocol steps were identical regardless of the sample/treatment type. Before analysis, samples were again filtered (10-kD cutoff; Centrifugal Devices NANOSEP). ATP, ADP, and AMP analytes were separately measured according to previously described LC-MS/MS methods (Paczia et al., 2012) using HPLC (1200 series; Agilent Technologies) coupled to a triple quadrupole mass spectrometer (API 4000; ABSciex) equipped with a TurboIon spray source. For details regarding MS operation, see Luo et al. (2007). When water controls were spiked with 10 µM ATP, summation of measured ATP, ADP, and AMP concentrations resulted in a mean concentration of 9.93 µM ATP ($n = 6$), demonstrating that arithmetic summation of ATP and its purine metabolites reproduces the original ATP concentration with high accuracy. Accordingly, "ATP concentrations" derived from LC-MS/MS report the sum of ATP, ADP, and AMP. Ion-pairing reversed-phase column chromatography (C18 Synergy hydro; Phenomenex) was used with eluent A (10 mM tributylamine aqueous solution and 5% methanol adjusted pH to 4.95 with 15 mM acetic acid) and eluent B (methanol) at 40°C. The following elution gradient was used: 2 min (100% A), 5 min (80% A), 8 min (80% A), 10 min (65% A), 14 min (0% A), 15 min (0% A), 15.5 min (100% A), and 18 min (100% A). The flow rate was set to 0.45 ml/min with 10-µl injection volume. Quantification was performed by isotope dilution mass spectrometry (Wu et al., 2005), adding ^{13}C-labeled internal standard obtained from batch cultivation of *Corynebacterium glutamicum* with uniformly ^{13}C-labeled glucose as the sole carbon source.

LC-MS/MS was carefully checked for cross-talk or false-positive detection of ATP originating from BzATP that was added in some experiments. For BzATP, stronger chromatographic retention was found showing clear baseline separation from ATP. Moreover, BzATP shows a unique MS/MS fragment pattern clearly separated from ATP with no interfering fragments; i.e., BzATP does not contaminate the mass trace of ATP or ATP fragments. However, the BzATP standard was found to contain ≤4% impurity of ATP, traces of ADP (below quantification limit), and no AMP. Measurement results were corrected accordingly, assuming maximum impurity.

Histology and immunochemistry

For immunochemistry of testicular cryosections, testes were fixed with 4% (wt/vol) paraformaldehyde (PFA) in Ca^{2+}-Mg^{2+}–free $PBS^{-/-}$ (10 mM, pH 7.4; ≥3 h for juvenile [P7] and ≥12 h for adult tissue; 4°C) and subsequently cryoprotected in $PBS^{-/-}$ containing 30% sucrose (≥24 h; 4°C). Samples were then embedded in Tissue Freezing Medium (Leica Biosystems), sectioned at 20 µm on a CM1950 cryostat (Leica Biosystems), and mounted on Superfrost Plus slides (Menzel). For blocking, sections were incubated in S_7 (1 h; RT; gentle agitation). Cryosections were then washed (2 × 5 min; S_9) and incubated with primary antibodies overnight (S_9; 4°C) in a dark humidified chamber. Primary antibodies were anti-DAZL (1:500; Abcam), anti-Sloα1 (extracellular; 1:500; Alomone Labs), anti-P2X4 (extracellular; 1:100, Alomone Labs), and anti-P2X7 (extracellular; 1:500; Alomone Labs). After washing in S_9 (5×, 10 min), sections were incubated in S_9 containing Alexa Fluor 488 goat anti–rabbit secondary antibody

(1:500; 1 h; RT; Thermo Fisher Scientific). Excess antibodies were removed by washing (3 × 5 min S_9, 2 × 5 min $PBS^{-/-}$).

For immunostaining of cultured spermatogonia, cells were washed ($PBS^{-/-}$) and fixed with 4% PFA in $PBS^{-/-}$ (45 min; RT). For blocking, cells were washed/incubated in S_8 (2 × 5 min, 1 × 60 min; RT). After incubation with the primary anti-DAZL antibody (1:200; 1 h; RT), cells were washed (3 × 5 min S_8) and incubated in $PBS^{-/-}$ containing Alexa Fluor 488 goat anti–rabbit secondary antibody (1:200; 45 min; RT). Excess antibodies were removed by washing (3 × 5 min $PBS^{-/-}$). For nuclear counterstaining, cells were incubated in $PBS^{-/-}$ containing DAPI (1:100; 15 min; RT; Thermo Fisher Scientific) and washed again in $PBS^{-/-}$.

Fluorescent images were taken using an upright fixed stage scanning confocal microscope (TCS SP5 DM6000 CFS; Leica Microsystems) equipped with a 20× 1.0 NA water immersion objective (HCX APO L; Leica Microsystems). To control for nonspecific staining and to demonstrate antibody specificity, we performed (a) antigen preadsorption controls and (b) experiments in which the primary antibodies were omitted in parallel with each procedure. Digital images were uniformly adjusted for brightness and contrast using Photoshop CS6 (Adobe Systems).

For immunoblotting, both testes and control tissues (i.e., brain, olfactory bulb, muscle, and HEK293T cells) were homogenized in lysis buffer (100 µl; 0.1% Triton X-100; 4°C) in the presence of Complete Mini protease inhibitor cocktail tablets (Roche). The homogenate was sonicated (5 s) and centrifuged for 10 min (4°C; 1,000 *g*). The supernatant was resuspended in lysis buffer. Protein concentration was determined and adjusted to 1.5 mg/ml by adding lysis buffer (BioPhotometer plus; Eppendorf). 30 µl Laemmli buffer (20% glycerol, 4% SDS, 125 mM Tris-HCl, and 0.02% bromophenol blue, pH 6.8) was added 1:1, and equal amounts of protein were fractionated by SDS-PAGE. Separated proteins were transferred using a Criterion Blotter wet-blotting system (Bio-Rad Laboratories). Membranes were washed, stained with Ponceau S to control for protein transfer, and again washed with TBST (61 mM Tris-HCl, 88 mM NaCl, and 0.1% Tween 20, pH 7.5). Blocking was performed in 5% nonfat dry milk/TBST overnight. Blots were then incubated in 2.5% nonfat dry milk/TBST (1 h, RT) with anti-Sloα1 (1:200) anti-P2X4 (1:200), and anti-P2X7 (1:200) antibodies. Membranes were then washed (4 × 15 min) in TBST and incubated with horseradish peroxidase–conjugated goat anti–rabbit IgG (Bio-Rad Laboratories; 45 min, RT, 1:5,000) in 2.5% nonfat dry milk/TBST. Blots were again washed in TBST (4 × 15 min), and antibody binding was detected using 2.5 ml Lumi-Light solution (Roche).

Scanning electron microscopy

For scanning electron microscopy, testes were dissected, and the seminiferous tubules were transferred into 100% ethanol and fast frozen by liquid nitrogen. Freeze-fracture of tissue samples was established using a scalpel. Fractured samples were then transferred into ethanol containing 0.5% glutaraldehyde (−80°C; 48 h). Next, glutaraldehyde concentration was sequentially increased to 2% (−80°C; 48 h), 4% (−20°C; 96 h), and 10% (4°C; 120 h). After chemical dehydration in hexamethyldisilazane and subsequent air drying (RT), samples were gold sputter coated to a thickness of ≤2 nm (8 min, 10 mA sputter current). Images were acquired using a Cambridge Stereoscan S604 electron microscope connected to an i-scan digitizer (ISS Group Services Ltd.).

Electrophysiology

We performed electrophysiological recordings from spermatogonia and Sertoli cells both in co-culture and in acute sections of seminiferous tubules. Cultured cells and slices were transferred to the stage of an inverse microscope (DMI 4000B, Leica Microsystems; co-cultures) or an upright fixed stage microscope (DM 6000FS, Leica Microsystems; slices), respectively. Microscopes were equipped for either phase contrast or infrared-optimized differential interference contrast (IR-DIC). Whereas cultured cells were observed using phase-contrast objectives (HCX PL FLUOTAR 20× 0.5 NA, 40× 0.6, and 63× 0.7; Leica Microsystems), acute sections were visualized using a 25× (HCX IRAPO L25×/0.95W) objective and a three-position magnification changer (0.35×, 1.25×, and 4.0×). Images were recorded using a cooled CCD camera (DFC365FX; Leica Microsystems). Samples were continuously superfused with S_1 (~3 ml/min; gravity flow; 23°C). Patch pipettes (5–7 MΩ) were pulled from borosilicate glass capillaries (1.50 mm OD/0.86 mm ID; Science Products) on a PC-10 micropipette puller (Narishige Instruments), fire polished (MF-830 Microforge; Narishige Instruments), and filled with pipette solution ($S_{5,6}$, depending on experimental design). In slice recordings, 20 µM Alexa Fluor488 hydrazide (Thermo Fisher Scientific) was routinely added to the pipette solution to allow online evaluation of cell morphology and post hoc three-dimensional reconstruction, respectively. An agar bridge (150 mM KCl) connected reference electrode and bath solution. An EPC-10 USB amplifier controlled by Patchmaster 2.67 software (HEKA) was used for data acquisition. We monitored and compensated pipette and membrane capacitance (C_{mem}) as well as series resistance. Treated, to a first approximation, as a "biological constant" with a value of ~1 µF/cm^2 (Gentet et al., 2000), C_{mem} values served as a proxy for the cell surface area and thus for normalization of current amplitudes (i.e., current density). Liquid junction potentials were calculated using

JPCalcW software (Barry, 1994) and corrected online. Signals were low-pass filtered (analogue 3- and 4-pole Bessel filters [−3 dB]; adjusted to 1/4 to 1/5 of the sampling rate [5–20 kHz; depending on protocol]). If not stated otherwise, holding potential (V_{hold}) was −40 mV. In some voltage-clamp experiments, leak currents were subtracted using a P/6 protocol at hyperpolarized V_{hold}. For clarity, few exemplary current traces (Figs. 4 B and 9 B) were subsequently processed using a "box-7" smoothing algorithm implemented in IGOR Pro 6.5 software (WaveMetrics). Moreover, electric artifacts resulting from valve switching were removed. All data were recorded at RT. Individual voltage step and ramp protocols are described in the Results section.

Data analysis

All data were obtained from independent experiments performed on at least 2 d. Individual numbers of cells/experiments (n) are denoted in the figure and/or captions. If not stated otherwise, results are presented as means ± SEM. Statistical analyses were performed using paired or unpaired t tests, one-way ANOVA with Tukey's HSD post hoc test, or the Fisher exact test (as dictated by data distribution and experimental design). Tests and corresponding p-values that report statistical significance ($\leq$0.05) are individually specified in the captions. Data were analyzed offline using FitMaster 2.67 (HEKA), IGOR Pro 6.5 (WaveMetrics), and Excel 2013 (15.0.4779.1001; Microsoft) software. Desensitization rates during successive ramp recordings (Fig. 6, B and D) were determined from linear regression fits to data plotted as current versus time (Fig. 6, C and E) in the presence of ATP and calculated as current reduction (%) over time (s; Fig. 6 G). Dose–response curves were fitted by the Hill equation.

Online supplemental material

Fig. S1 shows immunochemical analysis of channel/receptor protein expression in juvenile seminiferous cords. Fig. S2 shows dose-dependent inhibition of ATP responses by suramin in cultured Sertoli cells. Fig. S3 shows that posttranscriptional *P2rx2* gene silencing diminishes Sertoli cell ATP responses. Fig. S4 shows reduced BzATP sensitivity of Sertoli cell P2X receptors. Fig. S5 shows quantitative LC-MS/MS analysis of $[ATP]_{ex}$ in seminiferous epithelia. Online supplemental material is available at http://www.jgp.org/cgi/content/full/jgp.201611636/DC1.

RESULTS

A Sertoli cell–germ cell co-culture from immature seminiferous tissue maintains spermatogonia for physiological analysis

To investigate purinergic signaling mechanisms in spermatogonia, we first established Sertoli–germ cell co-cultures from testicular tissue of prepubescent mice. Seminiferous tubules were isolated at P7 to prevent culture contamination with meiotic or postmeiotic cell types (Bellvé et al., 1977; Creemers et al., 2002). When testicular tissue at P7 is compared by freeze-fracture electron microscopy with samples from adult animals (Fig. 1, A and B), the relatively homogenous composition of the smaller immature seminiferous cords becomes apparent (Fig. 1 B*i*). In corresponding cryosections (Fig. 1, C and D), immunochemical labeling of the spermatogonial marker protein DAZL (Deleted in AZoospermia-Like; VanGompel and Xu, 2011) reveals the expected circular staining in the basal compartment of adult seminiferous tubules (Fig. 1 C). In contrast, round DAZL-positive cells are diffusely distributed throughout the seminiferous cords in P7 mice (Fig. 1 D), confirming that most, if not all, germ cells in immature cords are spermatogonia. When Sertoli cell–germ cell co-cultures from immature seminiferous cords were performed according to established protocols (Veitinger et al., 2011; Hunter et al., 2012), apparent A_{single} and A_{paired} (Fig. 1 E) as well as larger clones of DAZL-positive $A_{aligned}$ spermatogonia (Fig. 1 F) resided on a confluent Sertoli cell feeder layer. Essentially all round cells in culture were labeled by the spermatogonial marker. Thus, the present co-culture allows maintenance of a relatively homogenous premeiotic germ cell population in vitro.

Spermatogonia are sensitive to purinergic stimulation over a broad concentration range

To address whether spermatogonia could be part of a paracrine purinergic signaling network (Praetorius and Leipziger, 2009), we performed whole-cell patch-clamp recordings from cultured germ cells (Fig. 2 A). For sample consistency, recordings were restricted to putative A_{single} and A_{paired} spermatogonia, which did not differ in any parameter investigated (i.e., both passive and active membrane properties). Spermatogonia exhibited a mean membrane capacitance (C_{mem}) of 15.8 ± 7.4 pF and an input resistance (R_{input}) of 1.24 ± 0.9 GΩ (means ± SD). When cells were exposed to 30 µM ATP at a negative holding potential (V_{hold} = −80 mV), we consistently recorded a fast-activating inward current in 51–78% of all spermatogonia (Fig. 2 A) throughout the experimental timeframe (DIV4–DIV7). Upon prolonged exposure (≥1 s), the current saturated and then monotonically declined in the presence of the stimulus (Fig. 2, A and B). This apparent desensitization was then examined in a multi-pulse paradigm (Fig. 2 C). When current amplitudes in response to a second stimulation were normalized to the initial signal, we observed essentially stable response magnitudes at interstimulus intervals (ISIs) >45 s. In contrast, a progressive decline in current amplitude emerged as a

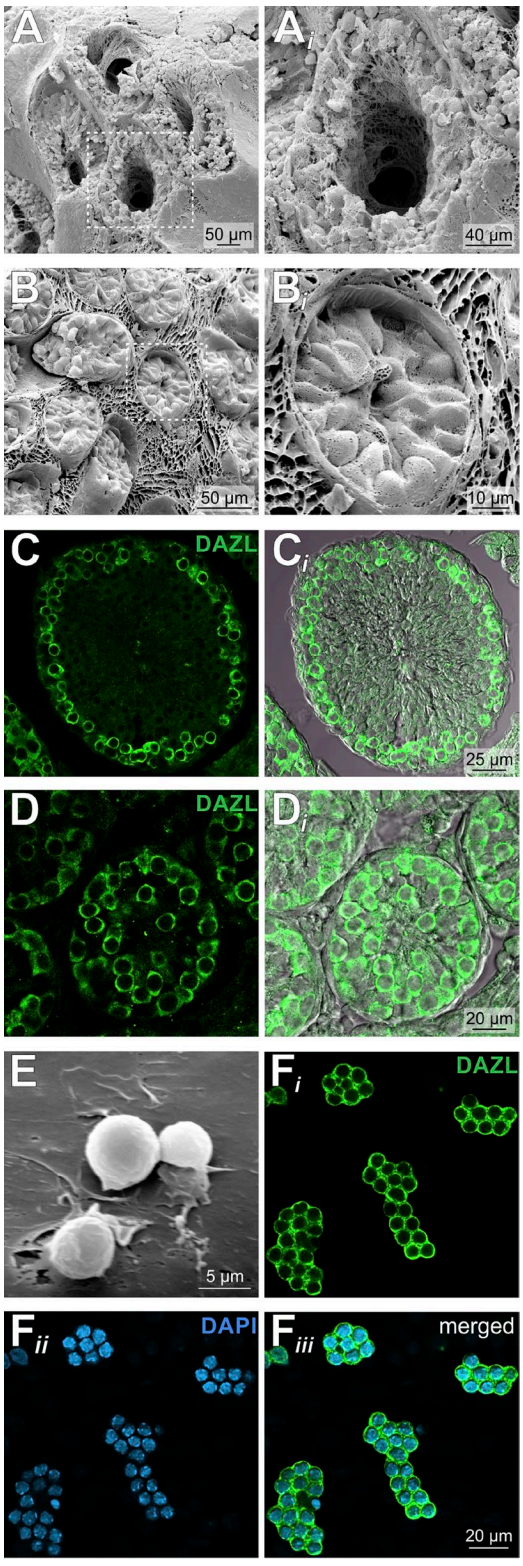

Figure 1. **A Sertoli cell–germ cell co-culture from immature seminiferous cords.** (A and B) Freeze-fracture scanning electron microscopy images of testicular tissue samples from adult (A) and prepubescent (B) mice. Areas delimited by dotted white rectangles are shown at higher magnification (A*i* and B*i*). In the adult tubules, the complex anatomy of the seminiferous epithelium and fully developed lumen become apparent, whereas the immature seminiferous cords exhibit a more homogenous cellular composition devoid of a lumen. (C and D) Confocal fluorescence images of immunostainings against DAZL, a marker of premeiotic germ cells. Cryosections from adult (C) and prepubescent (D) mice reveal DAZL-positive cells in the periphery of the adult seminiferous epithelium (C), whereas spermatogonia are scattered throughout the immature seminiferous cords (D) and appear to make up the only spherical seminiferous cell type at P7, as visualized in merged fluorescence and DIC micrographs (C*i* and D*i*). (E and F) Scanning electron microscopy (E) and confocal dual-channel fluorescence (F) images of Sertoli cell–germ cell co-cultures from seminiferous cords of prepubescent mice (P7). Relatively small spherical cells reside on a confluent flat layer of large Sertoli cells (E). Immunostaining against DAZL (F*i*) and nuclear counterstaining (DAPI; F*ii*) reveals spermatogonial marker expression in essentially all spherical cells. Note that cultured putative spermatogonia are found as single and paired cells (E) or as aligned groups of up to 16 cells (F).

function of reduced ISI. We therefore performed all subsequent recordings at an ISI of ≥1 min.

Next, we asked whether ATP sensitivity is dose dependent. At extracellular ATP concentrations ($[ATP]_{ex}$) of up to 300 µM, spermatogonia exhibited a sigmoidal dose–response relationship with a threshold $[ATP]_{ex}$ of ~3 µM and half-maximal activation at 13.5 µM (Fig. 2, D and E). Although we observed apparent saturation at $[ATP]_{ex}$ ≥100 µM, massively increased stimulus concentrations (≥1 mM) seemed to recruit a second low-affinity response mechanism. Notably, currents activated by these large concentrations lacked signs of desensitization (Fig. 2 D), supporting the notion of two independent signaling mechanisms that operate at opposite ends of the dose–response spectrum.

To examine the current–voltage relationship of "high-affinity" ATP-induced currents, we next challenged spermatogonia with 30 µM ATP at various membrane potentials (Fig. 2 F). Immediately activated currents reversed at ~0 mV and exhibited pronounced inward rectification (Fig. 2 G). Surprisingly, we observed an additional outward current that developed with considerable delay (Fig. 2 F) and reversed at approximately −80 mV (Fig. 2 G).

Together, our data reveal that cultured mouse spermatogonia express a distinct set of receptors and channels that confer both sensitivity and functional specificity in response to a universal auto/paracrine signal (i.e., ATP).

BK channels balance electrophysiological effects of ATP stimulation

Given the negative reversal potential (E_{rev}) of the ATP-dependent delayed conductance (and because measurements were conducted in symmetric Cl^- solutions), we hypothesized that this delayed current (I_{del}) is largely carried by K^+. To test this, we again recorded current–voltage curves in response to ATP (10 µM), replacing intracellular K^+ with Cs^+ (S_6; Fig. 3 A). Under these

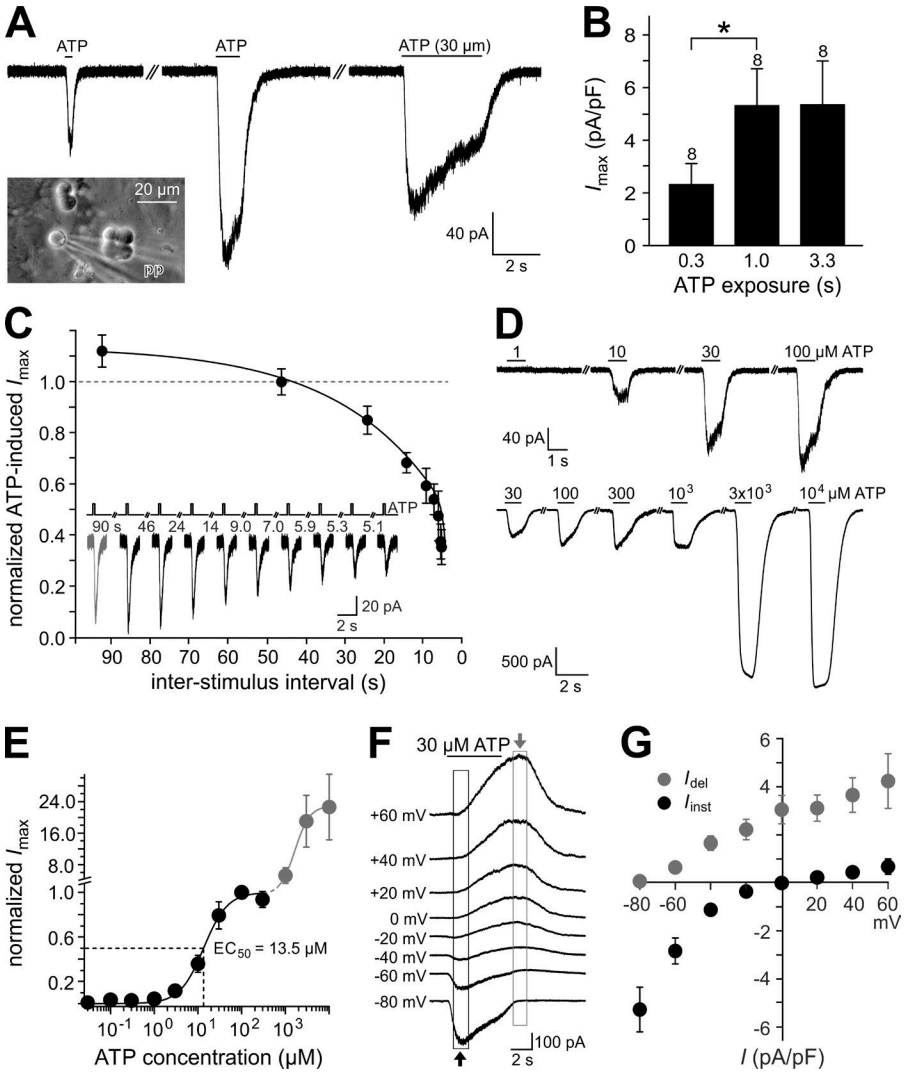

Figure 2. **Extracellular ATP stimulates spermatogonia.** (A) Original current traces from representative whole-cell patch-clamp recordings (V_{hold} = −80 mV; S_1, S_5) from a cultured mouse spermatogonium (DIV7) challenged with elevated $[ATP]_{ex}$ (30 µM) at increasing durations (0.3, 1.0, 3.3 s; horizontal bars). Prolonged stimulation (≥1 s) reveals current desensitization. (Inset) Phase-contrast micrograph depicting putative A_{single}, A_{paired}, and $A_{aligned}$ spermatogonia on a Sertoli cell feeder layer. The single spermatogonium is targeted by a patch pipette (pp). (B) Quantification of recordings as shown in A. Bar chart depicting peak current density measurements (mean ± SEM). Numbers of experiments are indicated above bars. Asterisk (*) denotes statistical significance, P = 0.01 (paired *t* test). (C) Representative whole-cell voltage-clamp traces (inset) and normalized mean peak response data (mean ± SEM) from multi-pulse stimulation experiments (V_{hold} = −80 mV; $[ATP]_{ex}$ = 100 µM/200 ms; *n* = 8). ISIs are progressively reduced from 90 s to 5.1 s. (D and E) Dose–response analysis of ATP-mediated whole-cell currents (V_{hold} = −80 mV; $[ATP]_{ex}$ = 0.03 µM to 10 mM; *n* = 5–50). Original traces from two recordings (D) and quantified data (E) reveal a double sigmoid curve on a logarithmic $[ATP]_{ex}$ scale. Individual data points in E are means ± SEM. Data are fit by the Hill equation. Dashed lines indicate the stimulus concentration that induces half-maximal activation of the high-affinity response (EC_{50} = 13.5 ± 1 µM; Hill coefficient η = 1.6 ± 0.2). Peak current amplitudes are normalized to each cell's response to 100 µM ATP. Note the discontinuous ordinate (//). (F) Representative traces illustrating a cell's ATP response profile (30 µM; 5 s; ISI = 180 s) at different V_{hold} (−80 to 60 mV; 20-mV increment). Note the biphasic response (arrows and open rectangles) consisting of an instantaneous current that is only observed at negative V_{hold} and a delayed outward current that increases with depolarization. (G) Current–voltage relationship of both the instantaneous (I_{inst}; black) and the delayed (I_{del}; gray) current. Individual data points depict mean current densities ± SEM (*n* = 18). Peak currents were measured during the boxed periods in F.

conditions, instantaneous ATP-mediated currents (I_{inst}) were still present in 40% of spermatogonia and appeared similar to control recordings (Fig. 2 G). In contrast, I_{del} was absent (Fig. 3, A–C), suggesting that this current is largely carried by K^+.

To identify the molecular correlate of I_{del}, we next determined the current's pharmacological profile (Fig. 3, D and E). First, 15 mM TEA strongly inhibited I_{del}. Second, I_{del} was essentially blocked when extracellular Ca^{2+} was reduced (110 nM), whereas I_{inst} was significantly increased under these conditions. Both Ca^{2+} dependence and TEA sensitivity are hallmarks of Ca^{2+}-activated BK channels (Marty, 1981; Pallotta et al., 1981; Yellen, 1984). If BK (Slo1) channels mediate I_{del}, the current should be blocked by the selective BK channel inhibitor iberiotoxin (Galvez et al., 1990). Indeed, iberiotoxin strongly reduced I_{del} without affecting I_{inst}. Moreover, an antibody against an extracellular epitope of the BK channel α-1 subunit (anti-Sloα1) specifically labeled spermatogonia-like cells in cryosections from P7 testes (Fig. S1, A–D). Our data thus indicate that, upon ATP exposure, spermatogonial BK channels are cooperatively activated by depolarization and increased cytoplasmic Ca^{2+}.

We next investigated how ATP stimulation translates into changes in membrane potential (V_{mem}). In current-clamp measurements, transient ATP exposure induced a biphasic V_{mem} response (Fig. 3, F and G). Fast depolarization was followed by gradual repolarization and transient hyperpolarization. Thus, ATP-dependent sequential activation of I_{inst} and I_{del} is mirrored by coun-

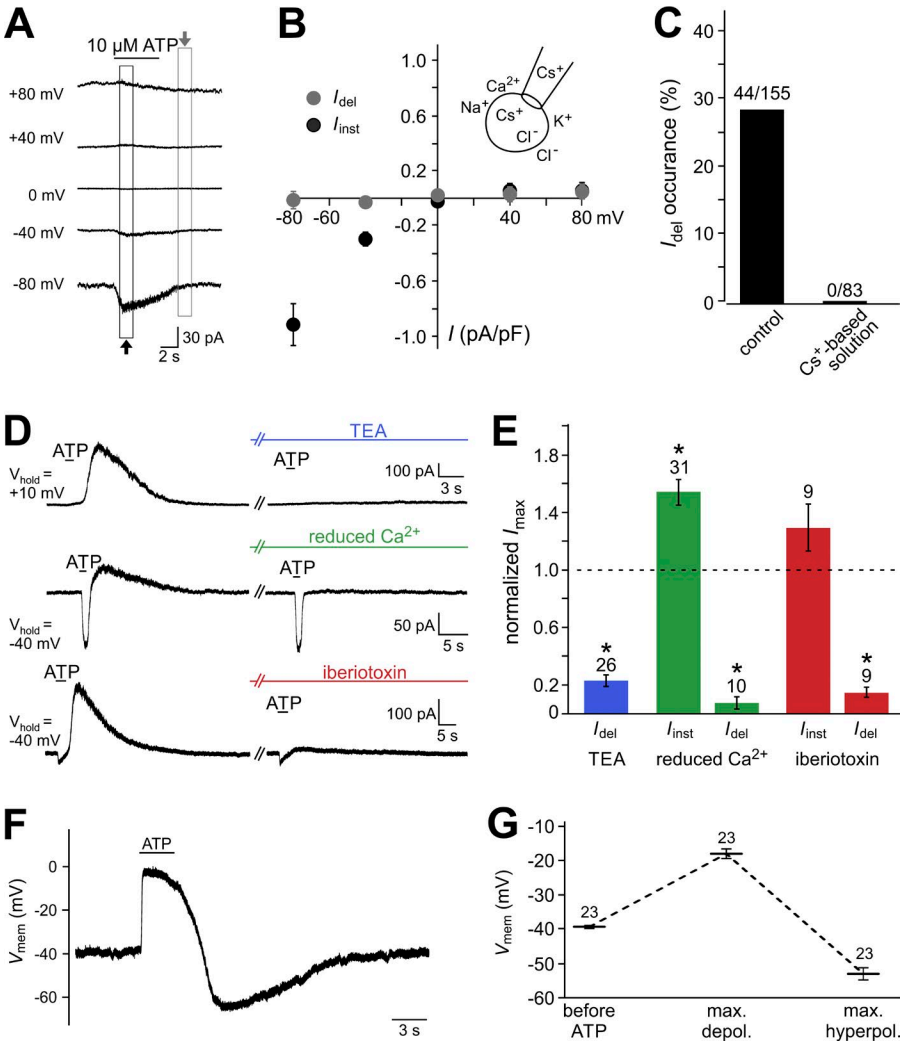

Figure 3. **Ca^{2+}-activated K^+ channels mediate I_{del}.** (A) Representative whole-cell ATP response profile (10 µM; 5 s; ISI = 180 s) at different V_{hold} (−80 to 80 mV; 40-mV increment) using Cs^+-based pipette solution (S_1, S_6). Arrows and corresponding open rectangles indicate the periods of I_{inst} and I_{del} measurements. (B) Current–voltage relationship of both I_{inst} (black) and I_{del} (gray). Individual data points depict mean current densities ± SEM (n = 6). Note that replacing intracellular K^+ with Cs^+ (inset) has no qualitative effect on I_{inst}, whereas I_{del} is essentially abolished. (C) Bar diagram showing the percentage of cells exhibiting I_{del} in response to ATP (10–100 µM) as a function of the pipette solution's dominant cation (K^+ or Cs^+). (D and E) Pharmacological profile of I_{del}. Representative traces from whole-cell voltage-clamp recordings (D) illustrate ATP-evoked responses (30 µM; ≥1 s) under control conditions (left) and in the presence of TEA (15 mM; V_{hold} = 10 mV; S_4), isomolar Ca^{2+} (110 nM; V_{hold} = −40 mV; S_3), or iberiotoxin (100 nM; V_{hold} = −40 mV; S_1), respectively (2 min preincubation; right). (E) Bar chart quantifying the effects of pharmacological treatment and reduction of extracellular Ca^{2+} on both I_{inst} and I_{del} (peak responses normalized to control conditions). Data are means ± SEM. Numbers of cells analyzed are indicated above bars. Asterisks (*) denote statistical significance, $P < 0.005$ (paired t tests comparing peak currents before [control] and during treatment). (F and G) ATP stimulation (100 µM; 3 s) affects spermatogonial V_{mem}. (F) Representative whole-cell current-clamp recording (S_1, S_5) illustrating a biphasic change in V_{mem}. From a resting potential of approximately −40 mV, ATP triggers rapid depolarization toward 0 mV (reversal potential of I_{inst}; B), which is followed by gradual repolarization and transient hyperpolarization. (G) Quantification of current-clamp recordings. Mean V_{mem} (±SEM; n = 23) is plotted at rest (without ATP; −39.4 ± 0.4 mV) as well as upon maximum de- and hyperpolarization (−18.1 ± 1.4 mV and −53.1 ± 1.7 mV), respectively. For comparison, resting V_{mem} was adjusted in a few cells to match −40 mV by small current injections.

teracting V_{mem} fluctuations between each current's characteristic E_{rev}. BK channels thus appear to narrow the temporal window of ATP-induced depolarization, and therefore, these channels constitute a potential mechanism of negative feedback control in spermatogonial purinergic signaling.

Spermatogonial high-affinity ATP responses are mediated by P2X4 receptors

We next aimed to identify the ion channel or channels underlying I_{inst}. Consistent with previous results (Veitinger et al., 2011), reverse transcription PCR–based expression profiling of all seven P2X receptor isoforms revealed transcripts for P2X2, P2X4, and P2X7 receptors in both Sertoli–germ cell co-cultures and juvenile testes at P7 (Fig. 4 A). Compared with other family members, P2X7 receptors exhibit substantially reduced ATP sensitivity (EC_{50} ≥300 µM [Chessell et al., 1998; Young et al., 2007; Casas-Pruneda et al., 2009]). Subsequent pharmacological/biophysical fingerprinting of I_{inst} was thus performed using low $[ATP]_{ex}$ (10 µM), Cs^+-based pipette solution (S_6), and V_{hold} close to E_K (−80 mV), preventing activation of both P2X7 and BK. First, spermatogonia were exposed to ATP in the presence of different concentrations of suramin, which inhibits P2X1, P2X2, and P2X3, but not P2X4 or P2X6 (Bo et al., 1995; Séguéla et al., 1996; King et al., 1997; Jones et al., 2004; Nicke et al., 2005). We confirmed drug efficacy by dose-dependent inhibition of P2X2-mediated currents recorded from cultured Sertoli cells (Fig. S2; Veitinger et al., 2011). In contrast, we never observed suramin-dependent inhibition of ATP responses in

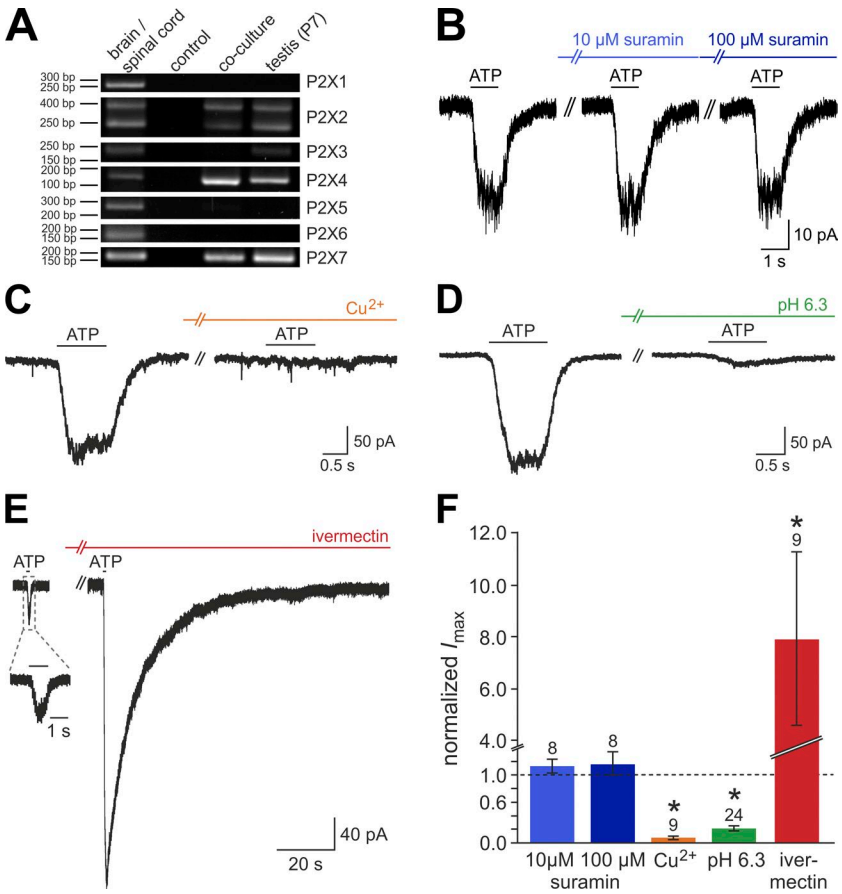

Figure 4. **P2X4 is a candidate mediator of the high-affinity ATP response in spermatogonia.** (A) Reverse transcription PCR reveals transcripts for *P2rx2*, *P2rx4*, and *P2rx7* in both Sertoli–germ cell co-cultures and whole testis preparations at P7. A faint band for *P2rx3*-encoding cDNA is only amplified from whole testis samples but not co-cultures. Primer pairs generate amplificates of 150–250 bp, respectively. cDNA from whole brain/spinal cord serves as positive control, whereas no template controls are devoid of detectable signals. (B–E) Exemplary whole-cell voltage-clamp recordings of ATP-induced currents (10 µM; 1 s; V_{hold} = −80 mV; S_1, S_6) under control conditions and during treatment with suramin (10 µM and 100 µM; B), extracellular Cu^{2+} (100 µM; C), reduced pH (6.3; D), and ivermectin (3 µM; E). Altered conditions were established for at least 60 s (preincubation). (F) Bar diagram (means ± SEM) depicting the quantitative analysis of experiments exemplified in B–E. Note the discontinuous ordinate (//). Numbers of cells tested are indicated above bars. Asterisks (*) denote statistical significance, $P \leq 0.01$ (paired *t* test).

spermatogonia (Fig. 4, B and F). Next, stimulations were performed in the presence of Cu^{2+}, which potentiates P2X2 (Xiong et al., 1999) but blocks P2X4 (Coddou et al., 2003). Spermatogonial ATP responses were essentially abolished by Cu^{2+} exposure (Fig. 4, C and F). Similar data resulted from extracellular acidification (pH 6.3; Fig. 4, D and F), which potentiates P2X2 (King et al., 1996; Veitinger et al., 2011) but inhibits P2X4 (Stoop et al., 1997). Finally, we stimulated spermatogonia in the absence and presence of ivermectin (Fig. 4, E and F), which selectively potentiates P2X4 (Khakh et al., 1999; Silberberg et al., 2007; Casas-Pruneda et al., 2009). The macrocyclic lactone mediated a dramatic increase in spermatogonial I_{inst}. Together, these data are most consistent with functional expression of homomeric P2X4 receptors in cultured mouse spermatogonia.

To verify the aforementioned conclusion, we immunochemically confirmed endogenous P2X4 expression in spermatogonia-like cells of juvenile seminiferous cords (Fig. S1, E–H), and we assessed the effect of selective P2X4 posttranscriptional gene silencing (knockdown) on spermatogonial ATP signaling by administration of siRNAs in vitro. Cells were transiently transfected with a fluorescent marker and either of two targeting siRNA constructs, a nontargeting negative control siRNA containing a nonspecific sequence or a construct selectively targeting P2X2, respectively (Fig. 5). Effective P2X4 knockdown by either targeting siRNA was confirmed by quantitative real-time PCR (Fig. 5 A). Relative to nontargeting siRNA controls, P2X4 transcript levels were reduced to 47 ± 4% (RNAi1) and 35 ± 5% (RNAi2), respectively. Readily identified by fluorescent labeling (Fig. 5 B), we next recorded I_{inst} from spermatogonia transfected with either siRNA construct (Fig. 5 C). Nontargeting negative control siRNA did not alter peak ATP responses. The same holds true for spermatogonia expressing P2X2-specific targeting constructs, for which we confirmed efficacy in Sertoli cell recordings (Fig. S3). In contrast, compared with both nontransfected cells and spermatogonia expressing nontargeting siRNA controls, selective P2X4 knockdown significantly reduced maximum I_{inst} (Fig. 5 D). Together, gene silencing experiments substantiate the notion that, at relatively low stimulus concentrations, ATP-dependent I_{inst} is predominantly, if not exclusively, mediated by P2X4 receptors.

P2X7 receptors mediate low-affinity ATP responses in spermatogonia

The two-step dose–response curve we observed when challenging spermatogonia with a broad range of $[ATP]_{ex}$ (1 µM to 10 mM; Fig. 2 F) strongly suggests a second low-affinity ATP response mechanism that operates at $[ATP]_{ex} \geq 300$ µM. Therefore, we next aimed to determine the molecular correlate of this low-affinity cur-

rent. Again, to avoid confounding BK channel currents, experiments were performed using Cs^+-based pipette solution (S_6). We first recorded currents induced by prolonged and repeated exposure to high $[ATP]_{ex}$ (1 mM; Fig. 6 A). In sharp contrast to the relatively small, desensitizing inward currents initiated by lower $[ATP]_{ex}$ (10 µM), high stimulus concentrations induced lasting currents that gradually increased during prolonged agonist exposure. By measuring I–V curves at a rate of 2 Hz before, during and after stimulation with either low $[ATP]_{ex}$ (100 µM; Fig. 6, B and C) or high $[ATP]_{ex}$ (1 mM; Fig. 6, D and E), several distinctive features of the low-affinity current emerged, i.e., (a) little rectification, (b) large amplitude, (c) slow development, and (d) no desensitization (Fig. 6, F and G). In concert with our expression profiling results (Fig. 4 A) and the considerably increased $[ATP]_{ex}$ required to activate the current, the aforementioned properties all indicate that P2X7 serves as the spermatogonial low-affinity ATP receptor (Surprenant et al., 1996; Chessell et al., 1998; Donnelly-Roberts et al., 2009). If so, the low-affinity current should (a) exhibit enhanced sensitivity when stimulated with the ~10-fold more potent agonist BzATP (Surprenant et al., 1996), (b) gradually increase upon repeated short stimulations (Yan et al., 2008), and (c) be insensitive to selective P2X4 knockdown. This is indeed the case (Fig. 7, A and B). When repeatedly exposed to brief pulses of intermediate $[ATP]_{ex}$ (300 µM), currents progressively decreased and mean amplitudes were strongly diminished in spermatogonia transfected with siRNA against P2X4. In contrast, successive stimulation with the same concentration of BzATP activated a larger current that increased with multiple stimulations and remained essentially unchanged by P2X4 knockdown. This effect, however, was restricted to spermatogonia because BzATP, as compared with ATP, proved much less potent when Sertoli cells were stimulated (Fig. S4), matching a previous report of reduced BzATP sensitivity of the P2X2 receptor (Evans et al., 1995).

Further evidence for functional expression of P2X7 in spermatogonia emerged from immunochemical analysis, pharmacological inhibition, and posttranscriptional gene silencing. Antibody staining against an extracellular P2X7 epitope revealed receptor expression in round cells of the juvenile seminiferous cord (Fig. S1, I–L). In whole-cell recordings, the selective P2X7 receptor antagonist A-438079 (McGaraughty et al., 2007) strongly reduced BzATP-mediated currents (Fig. 7, C and D), whereas responses to lower ATP concentrations were unaffected. Moreover, receptor knockdown significantly reduced the relative amount of P2X7 transcripts (Fig. 7 E) and had profound effects on current development upon prolonged ATP (1 mM) stimulation (Fig. 7 F). Although the initial desensitizing and inwardly rectifying current was largely unaffected by P2X7 gene silencing

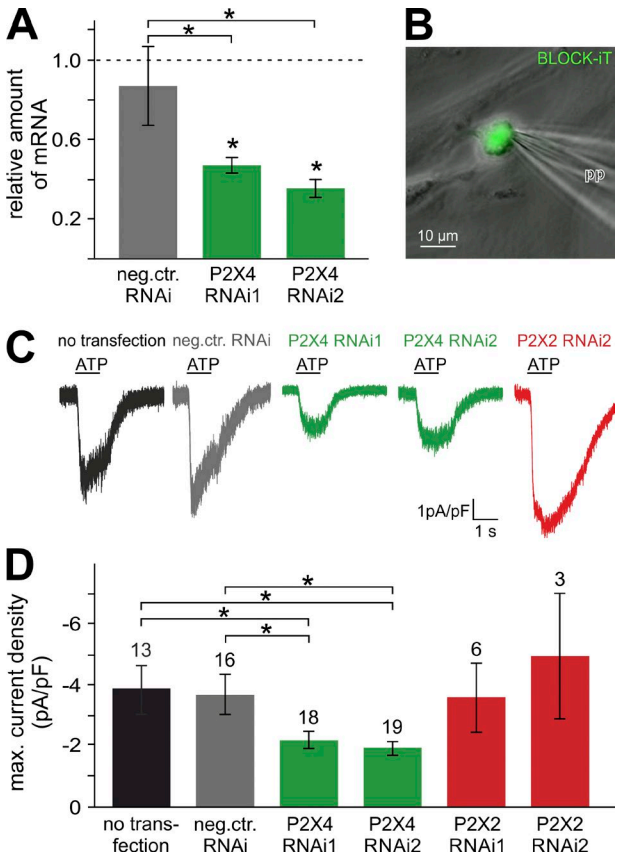

Figure 5. **Posttranscriptional gene silencing confirms P2X4 as the high-affinity spermatogonial ATP sensor.** (A) Bar chart quantifying siRNA-dependent selective knockdown of spermatogonial gene expression in vitro. When transfected with one of two siRNA constructs (green), knockdown of P2X4 expression was confirmed by quantitative real-time PCR. Transcript quantities (means ± SEM) are normalized to mRNA levels in untransfected spermatogonia and compared with cells treated with nontargeting siRNA controls (gray). Administration of both targeting siRNAs effectively reduced P2X4 transcription as compared with both untransfected spermatogonia and negative (nontargeting siRNA) controls. Asterisks (*) denote statistical significance, $P < 0.005$ (one-way ANOVA with Tukey's HSD post hoc test). (B) Merged DIC and fluorescence images of a single spermatogonium in culture that resides on Sertoli cells and is targeted by a patch pipette (pp). FITC-labeled BLOCK-iT fluorescent oligos allow identification of cotransfected cells by their fluorescence. (C) Original current density traces depicting representative whole-cell voltage-clamp recordings from spermatogonia exposed to ATP (300 µM; 1 s; $V_{hold} = -80$ mV; S_1, S_6). siRNA transfection, or the lack thereof (black), is color coded for nontargeting constructs (gray), two different targeting siRNAs (green), and a control construct targeting P2X2 expression (red). (D) Bar diagram quantifying the results exemplified in C. Data are means ± SEM. Numbers of experiments are denoted above bars. Color code as in C. Asterisks (*) indicate statistical significance, $P < 0.05$ (one-way ANOVA with Tukey's HSD post hoc test).

(Fig. 7, F, G, and I; and arrowhead in F), the slowly increasing essentially nonrectifying current that only saturated after tens of seconds (Fig. 7, F, H, and J; and

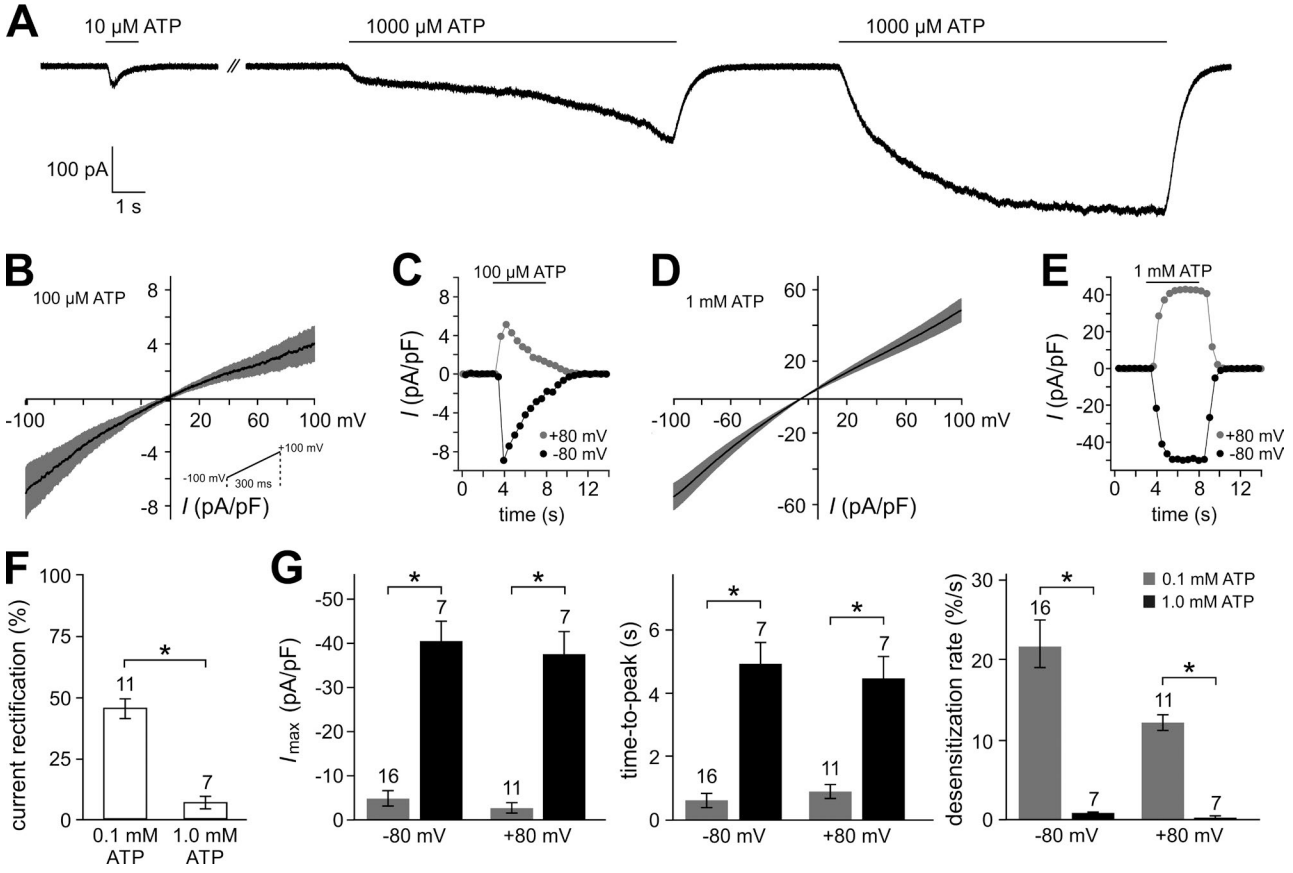

Figure 6. **Distinct biophysical signature of the low-affinity ATP response in spermatogonia.** (A) Representative whole-cell voltage-clamp recording (V_{hold} = −80 mV; S_1, S_6) comparing the rapidly desensitizing response to relatively low $[ATP]_{ex}$ (10 µM) with the gradually increasing current induced by prolonged exposure to high $[ATP]_{ex}$ (1 mM). (B–E) Current–voltage relationships (B and D) and current density time course (C and E) in response to 100 µM (n = 16) and 1 mM ATP (n = 7), respectively. (B, inset) Command voltage ramp, repeated at 2 Hz. I–V curves depict mean traces (black) and SEM (gray shadows). Data were corrected by digital offline subtraction of averaged leak controls recorded before stimulation. (C and E) Representative plots of current density measurements at −80 mV (black) and 80 mV (gray), respectively, over time. (F) Bar graph illustrating the difference in rectification as a function of stimulus concentration (100 µM vs. 1 mM ATP; mean ± SEM). Current rectification is calculated from individual ramp recordings (B and D) as the ratio of each cell's peak currents at 80 and −80 mV (I_{+80}/I_{-80}). Asterisk (*) denotes statistical significance, $P < 0.005$ (unpaired t test). (G) Bar diagrams comparing different current properties at 80 and −80 mV when activated by either 100 µM (gray) or 1 mM ATP (black). Plotted are peak current densities (I_{max}), rise time (time-to-peak), and desensitization rate during (%/s) ATP stimulation (mean ± SEM). Asterisks (*) indicate statistical significance, $P < 0.005$ (unpaired t tests).

asterisk in F) was substantially diminished in spermatogonia transfected with siRNA constructs targeting P2X7. Together, our findings suggest that P2X7 receptors are crucial mediators of the low-affinity ATP-dependent current in cultured mouse spermatogonia.

Multiple mechanisms of cellular ATP release in response to mechanical or biochemical stimulation have been discussed, including vesicular secretion (Bodin and Burnstock, 2001), active exocytosis of lysosomes (Zhang et al., 2007), and passive transport via connexin or pannexin hemichannels (Cotrina et al., 1998; Bao et al., 2004), large-conductance anion channels (Bell et al., 2003), or voltage-gated ATP-release channels (Taruno et al., 2013). Intriguingly, the P2X7 receptor has also been shown to function as an ATP-induced ATP release route (Pellegatti et al., 2005; Suadicani et al., 2006). Although FSH-dependent ATP release from Sertoli cells has been shown (Gelain et al., 2003, 2005) and ATP secretion from germ cells has been postulated (Lalevée et al., 1999), a potential self-enhancement mechanism via P2X7 receptors within the seminiferous epithelium has never been addressed. Therefore, we performed quantitative LC-MS/MS analysis of $[ATP]_{ex}$ in seminiferous tissue samples (Fig. S5). First, we controlled the method's accuracy by adding 10 µM ATP to either controls (water) or tissue samples (± a combination of different ectonucleotidase inhibitors). LC-MS/MS detected 9.93 ± 0.97 µM ATP in "no-tissue" controls (n = 6), suggesting a high degree of analytical accuracy. Seminiferous tissue that retained ectonucleotidase activity showed slightly, though not significantly reduced $[ATP]_{ex}$ (8.4 ± 1.88 µM), whereas broad range inhibi-

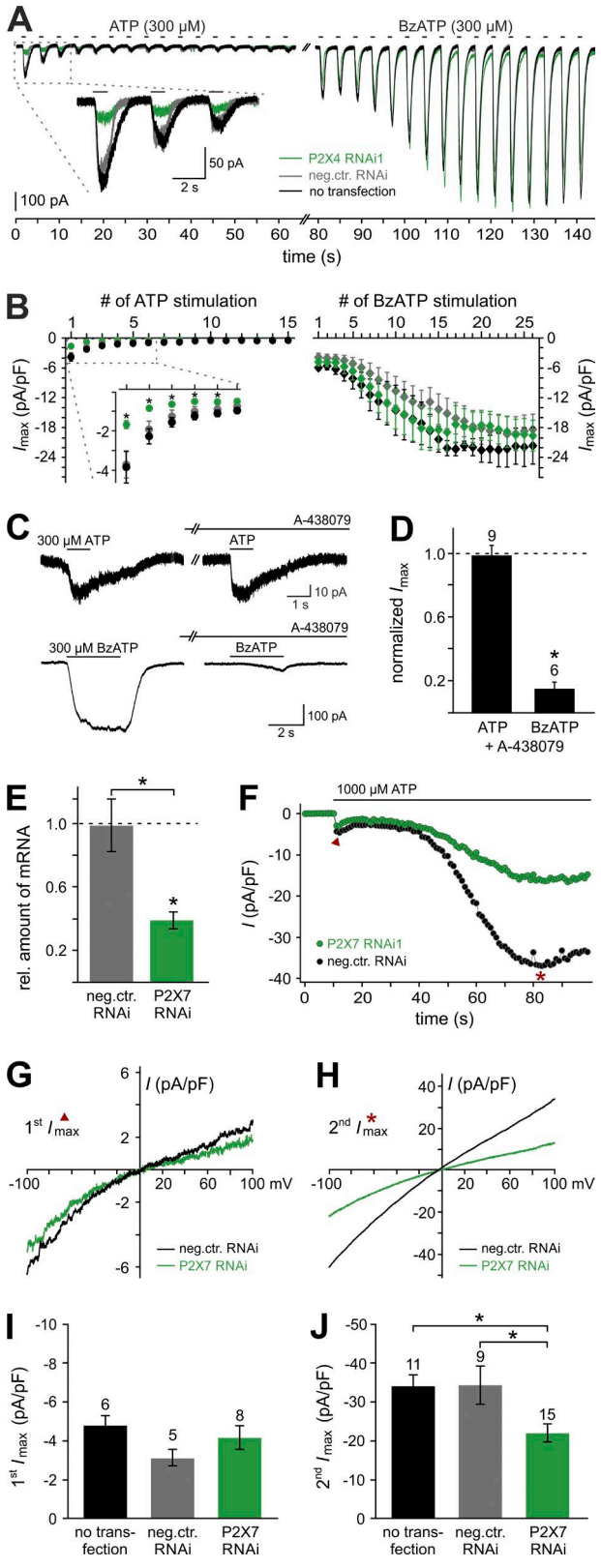

Figure 7. **P2X7 constitutes the low-affinity spermatogonial ATP sensor.** (A) Exemplary whole-cell voltage-clamp recordings of currents triggered by repetitive stimulation (1 s; ISI = 3 s; S_1, S_6) with ATP (300 µM; left) or BzATP (300 µM; right), respectively. Traces from untransfected spermatogonia (black) and cells transfected with either nontarget negative control siRNA (gray) or a construct targeting P2X4 (green) are overlaid. (B) Quantification of results from repetitive stimulation experiments as shown in A. Peak current densities (means ± SEM) are color coded and plotted as a function of stimulus repetition. Cells were analyzed under control conditions (n = 33/13 [ATP/BzATP]; black), after transfection with nontargeting siRNA (n = 16/23 [ATP/BzATP]; gray), and after P2X4 knockdown (n = 16/23 [ATP/BzATP]; green). Inset (left) shows the data delimited by the dashed rectangle at an increased scale. Asterisks (*) indicate statistical significance, $P < 0.05$ (one-way ANOVA with Tukey's HSD post hoc test). (C and D) Selective pharmacological inhibition of BzATP responses by 10 µM A-438079. (C) Representative whole-cell voltage-clamp recordings show individual responses to either 300 µM ATP (top) or 300 µM BzATP (bottom) in the absence or presence of the P2X7 receptor antagonist A-438079 (preincubation >60 s; S_1, S_6). (D) Bar chart quantifying the efficacy of A-438079 as a function of agonist type (ATP vs. BzATP). Data are means ± SEM; normalized to control conditions. Numbers of cells are indicated above bars. Asterisk (*) denotes statistical significance, $P < 0.005$ (paired t test). (E) When transfected with transcript-specific siRNA (green), posttranscriptional gene silencing of P2X7 expression is confirmed by quantitative PCR. Relative transcript levels (means ± SEM) are normalized to mRNA quantities in untransfected spermatogonia and compared with cells treated with nontargeting siRNA controls (gray). Asterisks (*) denote statistical significance, $P < 0.005$ (one-way ANOVA with Tukey's HSD post hoc test). (F) Representative current density plot over time. Each dot represents current measured at −80 mV obtained from sequential voltage ramps as in G and H. Data correspond to spermatogonia transfected with either targeting P2X7 siRNA (green) or a nontargeting control construct (black). When challenged with 1 mM ATP, a fast but relatively small inward current develops and shows a transient peak (first I_{max}; red arrowhead). After apparent desensitization, current amplitudes gradually increase over tens of seconds until a secondary maximum is reached (second I_{max}; red asterisk). (G and H) Exemplary current–voltage curves (−100 to 100 mV; 250 ms; 1 Hz repetition; S_1, S_6) in response to 1 mM ATP, corresponding to time points (first G vs. second H I_{max}) as indicated in F (red arrowhead and asterisk). Color code as for E and F. Data were corrected by digital offline subtraction of averaged leak controls recorded before stimulation. (I and J) Quantification of mean current densities measured at −80 mV at first (I) versus second (J) I_{max}; see F–H. Bar graphs display means ± SEM. Numbers of cells as shown above bars. Asterisks (*) indicate statistical significance, $P < 0.05$ (one-way ANOVA with Tukey's HSD post hoc test).

tion of ectonucleotidases resulted in slightly increased ATP levels (11.07 ± 0.76 µM; Fig. S5 A). Next, we compared the extracellular ATP content of seminiferous tissue samples (± ectonucleotidase inhibition) in the absence or presence of BzATP (Fig. S5 B). Control experiments showed (a) that BzATP does not contaminate the mass traces of ATP and its metabolites and (b) that LC-MS/MS results had to be corrected for up to 4% chemical impurity (not depicted). When stimulated with BzATP, tissue weight–corrected ATP levels massively increased by factors of 38 (−blocking agents) and 21 (+inhibitor cocktail), respectively. These results thus indicate that purinoceptor activation in seminiferous

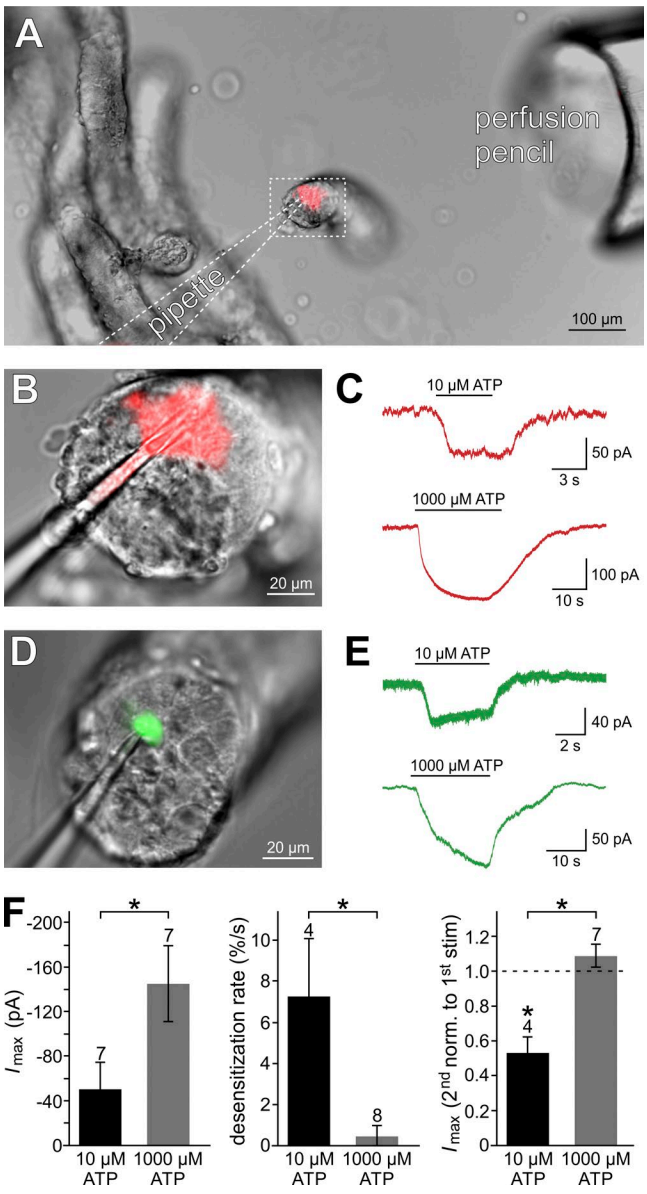

Figure 8. **Purinergic activation of both spermatogonia and Sertoli cells in acute seminiferous cord sections.** (A and B) Representative photomicrographs (merged IR-DIC and fluorescence images) illustrating the acute seminiferous cord slice preparation and experimental approach. (A) Overview of an exemplary section (200 µm) through agarose-embedded mouse seminiferous cords. Image shows typical experimental configurations of patch electrode (pipette; dotted lines) and perfusion pencil. Boxed area is shown at higher magnification in B. Whole-cell configuration and cell morphology are monitored by diffusion loading with a fluorophore (red). (C) Original whole-cell voltage-clamp recordings from a putative Sertoli cell (V_{hold} = −40 mV; S_1, S_5). Both low (10 µM; 5 s; top) and high (1 mM; 20 s; bottom) ATP concentrations induce gradually developing non-desensitizing inward currents. (D) Exemplary photomicrograph depicting a transverse section through a seminiferous cord (overlay of IR-DIC and fluorescence). A putative spermatogonium, diffusion loaded with fluorophore during whole-cell recording, is targeted by the patch pipette. (E) Original voltage-clamp recordings from a putative spermatogonium (V_{hold} = −40 mV; S_1, S_5) challenged with low (10 µM; 5 s; top) and high (1 mM; 20 s; bottom) ATP concentrations. (F) Quantitative analysis of current recordings from putative spermatogonia. Bar charts (means ± SEM) compare response parameters as a function of stimulus concentration (10 µM vs. 1 mM ATP). Diagrams depict peak current amplitudes (left), desensitization rate during prolonged stimulation (middle), and peak current desensitization according to a double-pulse stimulation paradigm (5 s; ISI = 60–240 s; right). Numbers of cells as shown above bars. Asterisks (*) indicate statistical significance, $P \leq 0.01$ (paired *t* tests).

tissue can trigger a self-enhancing ATP release pathway, possibly via spermatogonial P2X7 receptors.

An acute seminiferous cord preparation links in vitro findings to endogenous (electro)physiological profiles of male germ cells

So far, our data show that, in a Sertoli cell–germ cell co-culture, spermatogonia from juvenile mice detect elevations in $[ATP]_{ex}$ over a broad concentration range using both P2X4 and P2X7 receptors as well as BK channels that somewhat balance the ATP-dependent depolarization. To determine how these findings compare with data obtained in situ, we established an acute seminiferous cord slice preparation (Fig. 8 A) from juvenile mice. These sections preserve much of the tissue integrity, leaving the structure of, for example, Sertoli–germ cell junctions (Cheng and Mruk, 2002) or spermatogonial cytosolic bridges (Chiarini-Garcia and Russell, 2002) largely intact. Transverse section planes, in particular, allow for patch pipette access to both putative Sertoli cells (Fig. 8 B) and spermatogonia (Fig. 8 D) under visual control. Diffusion loading of target cells with a fluorophore during whole-cell recordings enables online visualization of cell morphology as well as post hoc three-dimensional reconstruction. ATP-induced currents from large irregularly shaped, columnar cells—putative Sertoli cells—displayed the nondesensitizing waveform of currents mediated by P2X2 receptors, irrespective of low or high $[ATP]_{ex}$ (Fig. 8 C). In contrast, recordings from smaller round cells—putative spermatogonia—revealed relatively rapid, desensitizing responses upon exposure to low $[ATP]_{ex}$ (10 µM) and slow, gradually increasing responses when challenged with high $[ATP]_{ex}$ (1 mM; Fig. 8 E). Comparative quantification of spermatogonial currents demonstrated dose-dependent peak responses as well as pronounced desensitization in response to low $[ATP]_{ex}$ versus no desensitization during stimulation with high $[ATP]_{ex}$ (Fig. 8 F). These data indicate that, in an intact environment, spermatogonia express at least two different ATP-dependent conductances that share kinetic hallmarks of P2X4 and P2X7 receptors.

If the observed in situ response profiles emerge from P2X2 receptor expression in Sertoli cells and/or expression of P2X4 and P2X7 receptors in spermatogonia,

respectively, ATP responses in acute sections should exhibit pharmacological characteristics similar to recordings from cells in Sertoli cell–germ cell co-culture. To address this, we recorded whole-cell currents from putative Sertoli cells and spermatogonia in response to both low and high $[ATP]_{ex}$ (10 µM and 1 mM, respectively) in the absence and presence of different P2X receptor antagonists (Fig. 9). Although suramin strongly inhibited low $[ATP]_{ex}$ responses in putative Sertoli cells, spermatogonial currents were essentially unaffected (Fig. 9, B and D). In contrast, the selective P2X7 receptor blocker A-438079 reduced spermatogonial responses to high $[ATP]_{ex}$, whereas the drug did not change signals in Sertoli cells (Fig. 9, C and D). Together, these findings support the endogenous functional expression of cell type–specific purinoceptor profiles within the premeiotic seminiferous epithelium. Our data also indicate that electrophysiological in vitro phenotypes are largely mirrored by both somatic and germ cells in an intact seminiferous cord preparation. Moreover, acute seminiferous cord/tubule slices provide an attractive experimental platform for direct analysis of diverse physiological processes in male reproductive biology.

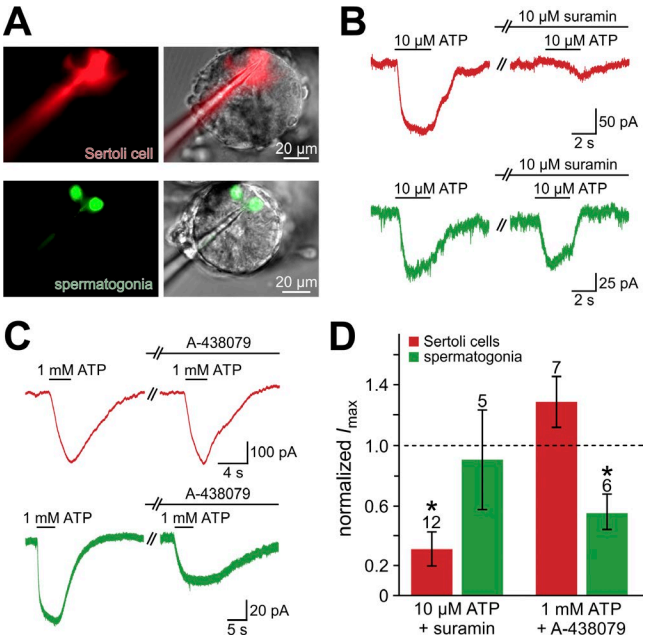

Figure 9. **Pharmacological profile of purinergic signals in the intact seminiferous epithelium.** (A) Representative fluorescence images (left) and merged photomicrographs (IR-DIC and fluorescence; right) of acute transverse seminiferous cord slices. A putative Sertoli cell (red; top) and two putative spermatogonia (green, bottom), likely connected by a cytosolic bridge, are diffusion loaded with fluorescent dyes during whole-cell patch-clamp recordings. (B and C) Representative whole-cell voltage-clamp recordings (V_{hold} = −40/−80 mV; S_1, S_5) from putative Sertoli cells (red) and spermatogonia (green). Cells are exposed for 3 s to low (10 µM; B) and high (1 mM; C) concentrations of ATP in the absence or presence of suramin (10 µM; B) or A-438079 (10 µM; C), respectively (preincubation = 120 s). (D) Bar graph depicting response amplitudes (means ± SEM) in the presence of suramin or A-438079. Signals are normalized to currents triggered before pharmacological treatment. Putative cell types are color coded. Numbers of cells as shown above bars. Asterisks (*) denote statistical significance, $P < 0.05$ (paired *t* tests).

DISCUSSION

Spermatogenesis, the complex, lifelong process of mass germ cell proliferation and transformation, is fundamental to reproduction and fertility, yet physiologically ill defined. Although extensive communication among and between Sertoli and germ cells coordinates spermatogenesis (Cheng and Mruk, 2002), the function of numerous paracrine factors that have been implicated in the seminiferous cycle remains elusive (Schlatt and Ehmcke, 2014). Here, we postulate a role for ATP in seminiferous epithelial communication, a key signaling component of several paracrine networks involved in other developmental processes (Abbracchio et al., 2009; Praetorius and Leipziger, 2009). In vitro and in situ experiments identify both P2X4 and P2X7 receptors as well as BK channels as critical mediators of purinergic responses in juvenile mouse spermatogonia.

Cell- and stage-specific testicular expression of several purinoceptor subunits has been reported in Sertoli cells (Veitinger et al., 2011), Leydig cells (Foresta et al., 1996; Antonio et al., 2009), postmeiotic germ cells (Glass et al., 2001), and mature spermatozoa (Navarro et al., 2011), albeit with somewhat contradictory results. An emerging concept implicates purinergic signaling mechanisms in paracrine control of gonadotropin effects on Sertoli and Leydig cells (Filippini et al., 1994; Meroni et al., 1998; Lalevée et al., 1999; Gelain et al., 2003, 2005), including, but not limited to, steroidogenesis and testosterone/17β-estradiol secretion (Foresta et al., 1996; Rossato et al., 2001). So far, the lack of an intact in situ preparation impeded functional analysis of the testicular purinergic signaling network in a physiological setting. The cellular complexity of the adult seminiferous epithelium as well as the lack of cell type–specific live cell markers have made it particularly difficult to analyze the distinct physiological properties of individual germ cell populations. The combination of a Sertoli–germ cell co-culture with acute seminiferous tubule sections from prepubescent mice overcomes this limitation as it allows a detailed physiological characterization of a defined germ cell population both in vitro and in situ. Our findings add spermatogonia to the seminiferous purinergic signaling circuit, suggesting that local $[ATP]_{ex}$ elevations will affect premeiotic male germ cells both electrophysiologically, by transient de- and hyperpolarization, and biochemically, by triggering substantial Ca^{2+} influx (unpublished data). Our data also indicate that one result of seminiferous

$[ATP]_{ex}$ elevation is paracrine signal amplification by increased ATP release, although the cellular identity of the ATP source or sources is currently unclear. The impact of this positive feedback on each testicular cell population will depend on the cell type– and stage-specific purinoceptor expression profile, as different isoforms vary dramatically with respect to agonist affinity, response kinetics, and desensitization (Coddou et al., 2011; Khakh and North, 2012).

The mechanism or mechanisms of ATP-induced ATP release remain elusive. ATP-induced cytosolic Ca^{2+} transients—potentially mediated by Ca^{2+} influx through P2X receptors, P2Y receptor-dependent Ca^{2+} release from storage organelles (Gelain et al., 2005; Veitinger et al., 2011), and/or activation of voltage-gated Ca^{2+} channels (Liévano et al., 1996)—could trigger exocytotic release of vesicles (Bodin and Burnstock, 2001) and other secretory granules (Zhang et al., 2007). Although nanomolar pericellular ATP concentrations are generally found in quiescent cells (Falzoni et al., 2013), the ATP concentration in secretory vesicles is claimed to be in the high millimolar range (Fields and Burnstock, 2006). However, alternative ATP release pathways, such as connexin or pannexin hemichannels (Cotrina et al., 1998; Bao et al., 2004), ATP-binding cassette transporters (Lohman et al., 2012), voltage-gated release channels (e.g., CALHM1 (Taruno et al., 2013), large-conductance anion channels (Bell et al., 2003), or even P2X7 receptors themselves (Pellegatti et al., 2005; Suadicani et al., 2006), cannot be excluded. Rapid enzymatic degradation by ectonucleotidases renders the half-life of extracellular ATP relatively short and thus narrows its paracrine radius to a few hundred micrometers (Fitz, 2007). Signal spread, however, is fast as ATP should diffuse ∼1 µm in <10 ms (Khakh, 2001). Given the spatial dimensions of the seminiferous tubule (Cheng and Mruk, 2002), ATP is thus ideally suited for a role as a fast local signal in paracrine testicular communication (Praetorius and Leipziger, 2009).

Which physiological roles might be included in the functional portfolio of testicular ATP signals? Evidently, the complexity and heterogeneity of the purinoceptor family allows for highly dynamic signaling over broad spatiotemporal scales. Short-term effects might include remodeling of the blood–testis barrier (Cheng and Mruk, 2002), synchronization of epithelial stage transitions (Heindel and Treinen, 1989; Syed and Hecht, 2002), control of bidirectional exchange between Sertoli and germ cells (McLachlan et al., 1995), and spontaneous epithelial Ca^{2+} oscillations (Sánchez-Cárdenas et al., 2012). Importantly, purinoceptor-dependent cytosolic Ca^{2+} elevations could also work on prolonged time scales, outlasting the short-term effects of the extracellular ATP surge (Khakh, 2001). For instance, Ca^{2+}-dependent recruitment of transcription factors and resulting long-term changes in gene expression could affect proliferation, differentiation, migration, and epithelial cell turnover. Because ATP release from apoptotic cells is well documented (Elliott et al., 2009) and because the P2X7 receptor, in particular, has been attributed a key role in cell death regulation (Surprenant et al., 1996), it is tempting to speculate that balancing the density-dependent germ cell death/survival ratio could also be a major function of the testicular purinergic signaling toolkit. Apoptosis is a vital process during spermatogenesis (Print and Loveland, 2000) as up to 75% of all germ cells undergo apoptosis under physiological conditions (Huckins, 1978).

With the exception of P2X1, which is critical for vas deferens contraction (Mulryan et al., 2000), no severe fertility deficits have been observed in P2X receptor–null mutants. In fact, phenotypic alterations in P2X knockout mice are rather subtle. Mice deficient for either P2X4 or P2X7 mostly show some immunological, cardiovascular, and/or neurological deficits as well as increased susceptibility to neuropathic pain (Coddou et al., 2011). However, given the versatile and often critical roles of purinoceptors in numerous physiological processes, deficiency compensation by alternative P2X isoform is likely to obscure the interpretation of gross phenotypic observations from knockout models.

In summary, we describe functional expression of P2X4 and P2X7 receptors as well as BK channels in immature male germ cells. Spermatogonia are thus equipped to respond to local testicular $[ATP]_{ex}$ elevations over a broad dynamic range with distinct and variable electrophysiological features, including negative feedback regulation of V_{mem} fluctuations by BK channel recruitment. In this scenario, ATP may function as a self-amplifying signal. Future studies will aim to determine the potential role or roles of purinoceptor signaling during meiosis and postmeiotic germ cell maturation.

ACKNOWLEDGMENTS

We thank Christa E. Müller for kindly providing reagents, Ingo Scholz (RWTH Aachen University) for helping with scanning electron microscopy, Annika Triller (University of Bonn) and Hanns Hatt (Ruhr-University Bochum) for help during the early stage of the project, Ralf Hausmann and Günther Schmalzing (RWTH Aachen University) for helpful comments and suggestions, and all members of the Spehr laboratory for stimulating discussions.

This work was funded by the Volkswagen Foundation (I/83533 to M. Spehr). M. Spehr is a Lichtenberg Professor of the Volkswagen Foundation.

The authors declare no competing financial interests.

Sharona E. Gordon served as editor.

Submitted: 7 June 2016
Accepted: 22 July 2016

REFERENCES

Abbracchio, M.P., G. Burnstock, A. Verkhratsky, and H. Zimmermann. 2009. Purinergic signalling in the nervous system: an overview. *Trends Neurosci.* 32:19–29. http://dx.doi.org/10.1016/j.tins.2008.10.001

Alexander, S.P.H., A. Mathie, and J.A. Peters. 2011. Guide to receptors and channels (GRAC), 5th edition. *Br. J. Pharmacol.* 164:S1–S324. http://dx.doi.org/10.1111/j.1476-5381.2011.01649_1.x

Antonio, L.S., R.R. Costa, M.D. Gomes, and W.A. Varanda. 2009. Mouse Leydig cells express multiple P2X receptor subunits. *Purinergic Signal.* 5:277–287. http://dx.doi.org/10.1007/s11302-008-9128-9

Bao, L., S. Locovei, and G. Dahl. 2004. Pannexin membrane channels are mechanosensitive conduits for ATP. *FEBS Lett.* 572:65–68. http://dx.doi.org/10.1016/j.febslet.2004.07.009

Barnard, E.A., G. Burnstock, and T.E. Webb. 1994. G protein-coupled receptors for ATP and other nucleotides: a new receptor family. *Trends Pharmacol. Sci.* 15:67–70. http://dx.doi.org/10.1016/0165-6147(94)90280-1

Barry, P.H. 1994. JPCalc, a software package for calculating liquid junction potential corrections in patch-clamp, intracellular, epithelial and bilayer measurements and for correcting junction potential measurements. *J. Neurosci. Methods.* 51:107–116. http://dx.doi.org/10.1016/0165-0270(94)90031-0

Bean, B.P. 1992. Pharmacology and electrophysiology of ATP-activated ion channels. *Trends Pharmacol. Sci.* 13:87–90. http://dx.doi.org/10.1016/0165-6147(92)90032-2

Bean, B.P., and D.D. Friel. 1990. ATP-activated channels in excitable cells. *Ion Channels.* 2:169–203. http://dx.doi.org/10.1007/978-1-4615-7305-0_5

Bell, P.D., J.-Y. Lapointe, R. Sabirov, S. Hayashi, J. Peti-Peterdi, K. Manabe, G. Kovacs, and Y. Okada. 2003. Macula densa cell signaling involves ATP release through a maxi anion channel. *Proc. Natl. Acad. Sci. USA.* 100:4322–4327. http://dx.doi.org/10.1073/pnas.0736323100

Bellvé, A.R., J.C. Cavicchia, C.F. Millette, D.A. O'Brien, Y.M. Bhatnagar, and M. Dym. 1977. Spermatogenic cells of the prepuberal mouse. Isolation and morphological characterization. *J. Cell Biol.* 74:68–85. http://dx.doi.org/10.1083/jcb.74.1.68

Bo, X., Y. Zhang, M. Nassar, G. Burnstock, and R. Schoepfer. 1995. A P2X purinoceptor cDNA conferring a novel pharmacological profile. *FEBS Lett.* 375:129–133. http://dx.doi.org/10.1016/0014-5793(95)01203-Q

Bodin, P., and G. Burnstock. 2001. Evidence that release of adenosine triphosphate from endothelial cells during increased shear stress is vesicular. *J. Cardiovasc. Pharmacol.* 38:900–908. http://dx.doi.org/10.1097/00005344-200112000-00012

Burnstock, G. 1990. Overview. Purinergic mechanisms. *Ann. N. Y. Acad. Sci.* 603:1–17. http://dx.doi.org/10.1111/j.1749-6632.1990.tb37657.x

Burnstock, G. 2008. Unresolved issues and controversies in purinergic signalling. *J. Physiol.* 586:3307–3312. http://dx.doi.org/10.1113/jphysiol.2008.155903

Casas-Pruneda, G., J.P. Reyes, G. Pérez-Flores, P. Pérez-Cornejo, and J. Arreola. 2009. Functional interactions between P2X4 and P2X7 receptors from mouse salivary epithelia. *J. Physiol.* 587:2887–2901. http://dx.doi.org/10.1113/jphysiol.2008.167395

Cheng, C.Y., and D.D. Mruk. 2002. Cell junction dynamics in the testis: Sertoli-germ cell interactions and male contraceptive development. *Physiol. Rev.* 82:825–874. http://dx.doi.org/10.1152/physrev.00009.2002

Chessell, I.P., J. Simon, A.D. Hibell, A.D. Michel, E.A. Barnard, and P.P.A. Humphrey. 1998. Cloning and functional characterisation of the mouse P2X7 receptor. *FEBS Lett.* 439:26–30. http://dx.doi.org/10.1016/S0014-5793(98)01332-5

Chiarini-Garcia, H., and L.D. Russell. 2002. Characterization of mouse spermatogonia by transmission electron microscopy. *Reproduction.* 123:567–577. http://dx.doi.org/10.1530/rep.0.1230567

Clapham, D.E. 2007. Calcium signaling. *Cell.* 131:1047–1058. http://dx.doi.org/10.1016/j.cell.2007.11.028

Coddou, C., B. Morales, J. González, M. Grauso, F. Gordillo, P. Bull, F. Rassendren, and J.P. Huidobro-Toro. 2003. Histidine 140 plays a key role in the inhibitory modulation of the P2X4 nucleotide receptor by copper but not zinc. *J. Biol. Chem.* 278:36777–36785. http://dx.doi.org/10.1074/jbc.M305177200

Coddou, C., Z. Yan, T. Obsil, J.P. Huidobro-Toro, and S.S. Stojilkovic. 2011. Activation and regulation of purinergic P2X receptor channels. *Pharmacol. Rev.* 63:641–683. http://dx.doi.org/10.1124/pr.110.003129

Cotrina, M.L., J.H. Lin, A. Alves-Rodrigues, S. Liu, J. Li, H. Azmi-Ghadimi, J. Kang, C.C. Naus, and M. Nedergaard. 1998. Connexins regulate calcium signaling by controlling ATP release. *Proc. Natl. Acad. Sci. USA.* 95:15735–15740. http://dx.doi.org/10.1073/pnas.95.26.15735

Creemers, L.B., K. den Ouden, A.M.M. van Pelt, and D.G. de Rooij. 2002. Maintenance of adult mouse type A spermatogonia in vitro: influence of serum and growth factors and comparison with prepubertal spermatogonial cell culture. *Reproduction.* 124:791–799. http://dx.doi.org/10.1530/rep.0.1240791

Donnelly-Roberts, D.L., M.T. Namovic, P. Han, and M.F. Jarvis. 2009. Mammalian P2X7 receptor pharmacology: comparison of recombinant mouse, rat and human P2X7 receptors. *Br. J. Pharmacol.* 157:1203–1214. http://dx.doi.org/10.1111/j.1476-5381.2009.00233.x

Elliott, M.R., F.B. Chekeni, P.C. Trampont, E.R. Lazarowski, A. Kadl, S.F. Walk, D. Park, R.I. Woodson, M. Ostankovich, P. Sharma, et al. 2009. Nucleotides released by apoptotic cells act as a find-me signal to promote phagocytic clearance. *Nature.* 461:282–286. http://dx.doi.org/10.1038/nature08296

Evans, R.J., C. Lewis, G. Buell, S. Valera, R.A. North, and A. Surprenant. 1995. Pharmacological characterization of heterologously expressed ATP-gated cation channels (P2x purinoceptors). *Mol. Pharmacol.* 48:178–183.

Fakler, B., and J.P. Adelman. 2008. Control of K_{Ca} channels by calcium nano/microdomains. *Neuron.* 59:873–881. http://dx.doi.org/10.1016/j.neuron.2008.09.001

Falzoni, S., G. Donvito, and F. Di Virgilio. 2013. Detecting adenosine triphosphate in the pericellular space. *Interface Focus.* 3:20120101. http://dx.doi.org/10.1098/rsfs.2012.0101

Fields, R.D., and G. Burnstock. 2006. Purinergic signalling in neuron-glia interactions. *Nat. Rev. Neurosci.* 7:423–436. http://dx.doi.org/10.1038/nrn1928

Filippini, A., A. Riccioli, P. De Cesaris, R. Paniccia, A. Teti, M. Stefanini, M. Conti, and E. Ziparo. 1994. Activation of inositol phospholipid turnover and calcium signaling in rat Sertoli cells by P2-purinergic receptors: modulation of follicle-stimulating hormone responses. *Endocrinology.* 134:1537–1545.

Fitz, J.G. 2007. Regulation of cellular ATP release. *Trans. Am. Clin. Climatol. Assoc.* 118:199–208.

Foresta, C., M. Rossato, P. Bordon, and F. Di Virgilio. 1995. Extracellular ATP activates different signalling pathways in rat Sertoli cells. *Biochem. J.* 311:269–274. http://dx.doi.org/10.1042/bj3110269

Foresta, C., M. Rossato, A. Nogara, F. Gottardello, P. Bordon, and F. Di Virgilio. 1996. Role of P2-purinergic receptors in rat Leydig cell steroidogenesis. *Biochem. J.* 320:499–504. http://dx.doi.org/10.1042/bj3200499

Galvez, A., G. Gimenez-Gallego, J.P. Reuben, L. Roy-Contancin, P. Feigenbaum, G.J. Kaczorowski, and M.L. Garcia. 1990.

Purification and characterization of a unique, potent, peptidyl probe for the high conductance calcium-activated potassium channel from venom of the scorpion Buthus tamulus. *J. Biol. Chem.* 265:11083–11090.

Gelain, D.P., L.F. de Souza, and E.A. Bernard. 2003. Extracellular purines from cells of seminiferous tubules. *Mol. Cell. Biochem.* 245:1–9. http://dx.doi.org/10.1023/A:1022857608849

Gelain, D.P., E.A. Casali, R.B. de Oliveira, L.F. de Souza, F. Barreto, F. Dal-Pizzol, and J.C. Moreira. 2005. Effects of follicle-stimulating hormone and vitamin A upon purinergic secretion by rat Sertoli cells. *Mol. Cell. Biochem.* 278:185–194. http://dx.doi.org/10.1007/s11010-005-7500-4

Gentet, L.J., G.J. Stuart, and J.D. Clements. 2000. Direct measurement of specific membrane capacitance in neurons. *Biophys. J.* 79:314–320. http://dx.doi.org/10.1016/S0006-3495(00)76293-X

Glass, R., M. Bardini, T. Robson, and G. Burnstock. 2001. Expression of nucleotide P2X receptor subtypes during spermatogenesis in the adult rat testis. *Cells Tissues Organs (Print).* 169:377–387. http://dx.doi.org/10.1159/000047905

Heindel, J.J., and K.A. Treinen. 1989. Physiology of the male reproductive system: endocrine, paracrine and autocrine regulation. *Toxicol. Pathol.* 17:411–445. http://dx.doi.org/10.1177/019262338901700219

Hess, R.A., and L.R. de Franca. 2008. Spermatogenesis and cycle of the seminiferous epithelium. *In* Molecular Mechanisms in Spermatogenesis. C.Y. Cheng, editor. Spinger-Verlag, New York. 1–15.

Huckins, C. 1978. The morphology and kinetics of spermatogonial degeneration in normal adult rats: an analysis using a simplified classification of the germinal epithelium. *Anat. Rec.* 190:905–926. http://dx.doi.org/10.1002/ar.1091900410

Hunter, D., R. Anand-Ivell, S. Danner, and R. Ivell. 2012. Models of in vitro spermatogenesis. *Spermatogenesis.* 2:32–43. http://dx.doi.org/10.4161/spmg.19383

Iwanami, Y., T. Kobayashi, M. Kato, M. Hirabayashi, and S. Hochi. 2006. Characteristics of rat round spermatids differentiated from spermatogonial cells during co-culture with Sertoli cells, assessed by flow cytometry, microinsemination and RT-PCR. *Theriogenology.* 65:288–298. http://dx.doi.org/10.1016/j.theriogenology.2005.04.025

Jan, S.Z., G. Hamer, S. Repping, D.G. de Rooij, A.M.M. van Pelt, and T.L. Vormer. 2012. Molecular control of rodent spermatogenesis. *Biochim. Biophys. Acta.* 1822:1838–1850. http://dx.doi.org/10.1016/j.bbadis.2012.02.008

Jarvis, M.F., and B.S. Khakh. 2009. ATP-gated P2X cation-channels. *Neuropharmacology.* 56:208–215. http://dx.doi.org/10.1016/j.neuropharm.2008.06.067

Jones, C.A., C. Vial, L.A. Sellers, P.P.A. Humphrey, R.J. Evans, and I.P. Chessell. 2004. Functional regulation of $P2X_6$ receptors by *N*-linked glycosylation: identification of a novel αβ-methylene ATP-sensitive phenotype. *Mol. Pharmacol.* 65:979–985. http://dx.doi.org/10.1124/mol.65.4.979

Khakh, B.S. 2001. Molecular physiology of P2X receptors and ATP signalling at synapses. *Nat. Rev. Neurosci.* 2:165–174. http://dx.doi.org/10.1038/35058521

Khakh, B.S., and R.A. North. 2012. Neuromodulation by extracellular ATP and P2X receptors in the CNS. *Neuron.* 76:51–69. http://dx.doi.org/10.1016/j.neuron.2012.09.024

Khakh, B.S., W.R. Proctor, T.V. Dunwiddie, C. Labarca, and H.A. Lester. 1999. Allosteric control of gating and kinetics at $P2X_4$ receptor channels. *J. Neurosci.* 19:7289–7299.

King, B.F., L.E. Ziganshina, J. Pintor, and G. Burnstock. 1996. Full sensitivity of P_{2X2} purinoceptor to ATP revealed by changing extracellular pH. *Br. J. Pharmacol.* 117:1371–1373. http://dx.doi.org/10.1111/j.1476-5381.1996.tb15293.x

King, B.F., S.S. Wildman, L.E. Ziganshina, J. Pintor, and G. Burnstock. 1997. Effects of extracellular pH on agonism and antagonism at a recombinant P2X2 receptor. *Br. J. Pharmacol.* 121:1445–1453. http://dx.doi.org/10.1038/sj.bjp.0701286

Ko, W.H., C.L. Au, and C.Y. Yip. 2003. Multiple purinergic receptors lead to intracellular calcium increases in cultured rat Sertoli cells. *Life Sci.* 72:1519–1535. http://dx.doi.org/10.1016/S0024-3205(02)02410-4

Kolasa, A., K. Misiakiewicz, M. Marchlewicz, and B. Wiszniewska. 2012. The generation of spermatogonial stem cells and spermatogonia in mammals. *Reprod. Biol.* 12:5–23. http://dx.doi.org/10.1016/S1642-431X(12)60074-6

Lalevée, N., C. Rogier, F. Becq, and M. Joffre. 1999. Acute effects of adenosine triphosphates, cyclic 3′,5′-adenosine monophosphates, and follicle-stimulating hormone on cytosolic calcium level in cultured immature rat Sertoli cells. *Biol. Reprod.* 61:343–352. http://dx.doi.org/10.1095/biolreprod61.2.343

Lee, S.Y., A. Fiene, W. Li, T. Hanck, K.A. Brylev, V.E. Fedorov, J. Lecka, A. Haider, H.J. Pietzsch, H. Zimmermann, et al. 2015. Polyoxometalates—potent and selective ecto-nucleotidase inhibitors. *Biochem. Pharmacol.* 93:171–181. http://dx.doi.org/10.1016/j.bcp.2014.11.002

Liévano, A., C.M. Santi, C.J. Serrano, C.L. Treviño, A.R. Bellvé, A. Hernández-Cruz, and A. Darszon. 1996. T-type Ca^{2+} channels and α_{1E} expression in spermatogenic cells, and their possible relevance to the sperm acrosome reaction. *FEBS Lett.* 388:150–154. http://dx.doi.org/10.1016/0014-5793(96)00515-7

Lohman, A.W., M. Billaud, and B.E. Isakson. 2012. Mechanisms of ATP release and signalling in the blood vessel wall. *Cardiovasc. Res.* 95:269–280. http://dx.doi.org/10.1093/cvr/cvs187

Luo, B., K. Groenke, R. Takors, C. Wandrey, and M. Oldiges. 2007. Simultaneous determination of multiple intracellular metabolites in glycolysis, pentose phosphate pathway and tricarboxylic acid cycle by liquid chromatography-mass spectrometry. *J. Chromatogr. A.* 1147:153–164. http://dx.doi.org/10.1016/j.chroma.2007.02.034

Marty, A. 1981. Ca-dependent K channels with large unitary conductance in chromaffin cell membranes. *Nature.* 291:497–500. http://dx.doi.org/10.1038/291497a0

McGaraughty, S., K.L. Chu, M.T. Namovic, D.L. Donnelly-Roberts, R.R. Harris, X.F. Zhang, C.-C. Shieh, C.T. Wismer, C.Z. Zhu, D.M. Gauvin, et al. 2007. P2X7-related modulation of pathological nociception in rats. *Neuroscience.* 146:1817–1828. http://dx.doi.org/10.1016/j.neuroscience.2007.03.035

McLachlan, R.I., N.G. Wreford, D.M. Robertson, and D.M. de Kretser. 1995. Hormonal control of spermatogenesis. *Trends Endocrinol. Metab.* 6:95–101. http://dx.doi.org/10.1016/1043-2760(94)00215-P

Meroni, S.B., D.F. Cánepa, E.H. Pellizzari, H.F. Schteingart, and S.B. Cigorraga. 1998. Effects of purinergic agonists on aromatase and gamma-glutamyl transpeptidase activities and on transferrin secretion in cultured Sertoli cells. *J. Endocrinol.* 157:275–283. http://dx.doi.org/10.1677/joe.0.1570275

Mulryan, K., D.P. Gitterman, C.J. Lewis, C. Vial, B.J. Leckie, A.L. Cobb, J.E. Brown, E.C. Conley, G. Buell, C.A. Pritchard, and R.J. Evans. 2000. Reduced vas deferens contraction and male infertility in mice lacking P2X1 receptors. *Nature.* 403:86–89. http://dx.doi.org/10.1038/47495

Navarro, B., K. Miki, and D.E. Clapham. 2011. ATP-activated P2X2 current in mouse spermatozoa. *Proc. Natl. Acad. Sci. USA.* 108:14342–14347. http://dx.doi.org/10.1073/pnas.1111695108

Nicke, A., D. Kerschensteiner, and F. Soto. 2005. Biochemical and functional evidence for heteromeric assembly of P2X1 and P2X4

subunits. *J. Neurochem.* 92:925–933. http://dx.doi.org/10.1111/j.1471-4159.2004.02939.x

Paczia, N., A. Nilgen, T. Lehmann, J. Gätgens, W. Wiechert, and S. Noack. 2012. Extensive exometabolome analysis reveals extended overflow metabolism in various microorganisms. *Microb. Cell Fact.* 11:122. http://dx.doi.org/10.1186/1475-2859-11-122

Pallotta, B.S., K.L. Magleby, and J.N. Barrett. 1981. Single channel recordings of Ca^{2+}-activated K^+ currents in rat muscle cell culture. *Nature.* 293:471–474. http://dx.doi.org/10.1038/293471a0

Pellegatti, P., S. Falzoni, P. Pinton, R. Rizzuto, and F. Di Virgilio. 2005. A novel recombinant plasma membrane-targeted luciferase reveals a new pathway for ATP secretion. *Mol. Biol. Cell.* 16:3659–3665. http://dx.doi.org/10.1091/mbc.E05-03-0222

Poletto Chaves, L.A., E.P. Pontelli, and W.A. Varanda. 2006. P2X receptors in mouse Leydig cells. *Am. J. Physiol. Cell Physiol.* 290:C1009–C1017. http://dx.doi.org/10.1152/ajpcell.00506.2005

Praetorius, H.A., and J. Leipziger. 2009. ATP release from non-excitable cells. *Purinergic Signal.* 5:433–446. http://dx.doi.org/10.1007/s11302-009-9146-2

Print, C.G., and K.L. Loveland. 2000. Germ cell suicide: new insights into apoptosis during spermatogenesis. *BioEssays.* 22:423–430. http://dx.doi.org/10.1002/(SICI)1521-1878(200005)22:5<423::AID-BIES4>3.0.CO;2-0

Rossato, M., M. Merico, A. Bettella, P. Bordon, and C. Foresta. 2001. Extracellular ATP stimulates estradiol secretion in rat Sertoli cells in vitro: modulation by external sodium. *Mol. Cell. Endocrinol.* 178:181–187. http://dx.doi.org/10.1016/S0303-7207(01)00426-9

Rudge, S.A., P.J. Hughes, G.R. Brown, R.H. Michell, and C.J. Kirk. 1995. Inositol lipid-mediated signalling in response to endothelin and ATP in the mammalian testis. *Mol. Cell. Biochem.* 149-150:161–174. http://dx.doi.org/10.1007/BF01076574

Sánchez-Cárdenas, C., A. Guerrero, C.L. Treviño, A. Hernández-Cruz, and A. Darszon. 2012. Acute slices of mice testis seminiferous tubules unveil spontaneous and synchronous Ca^{2+} oscillations in germ cell clusters. *Biol. Reprod.* 87:92. http://dx.doi.org/10.1095/biolreprod.112.100255

Schlatt, S., and J. Ehmcke. 2014. Regulation of spermatogenesis: an evolutionary biologist's perspective. *Semin. Cell Dev. Biol.* 29:2–16. http://dx.doi.org/10.1016/j.semcdb.2014.03.007

Séguéla, P., A. Haghighi, J.-J. Soghomonian, and E. Cooper. 1996. A novel neuronal P2x ATP receptor ion channel with widespread distribution in the brain. *J. Neurosci.* 16:448–455.

Silberberg, S.D., M. Li, and K.J. Swartz. 2007. Ivermectin interaction with transmembrane helices reveals widespread rearrangements during opening of P2X receptor channels. *Neuron.* 54:263–274. http://dx.doi.org/10.1016/j.neuron.2007.03.020

Stoop, R., A. Surprenant, and R.A. North. 1997. Different sensitivities to pH of ATP-induced currents at four cloned P2X receptors. *J. Neurophysiol.* 78:1837–1840.

Suadicani, S.O., C.F. Brosnan, and E. Scemes. 2006. $P2X_7$ receptors mediate ATP release and amplification of astrocytic intercellular Ca^{2+} signaling. *J. Neurosci.* 26:1378–1385. http://dx.doi.org/10.1523/JNEUROSCI.3902-05.2006

Surprenant, A., F. Rassendren, E. Kawashima, R.A. North, and G. Buell. 1996. The cytolytic P2Z receptor for extracellular ATP identified as a P2X receptor (P2X7). *Science.* 272:735–738. http://dx.doi.org/10.1126/science.272.5262.735

Syed, V., and N.B. Hecht. 2002. Disruption of germ cell-Sertoli cell interactions leads to spermatogenic defects. *Mol. Cell. Endocrinol.* 186:155–157. http://dx.doi.org/10.1016/S0303-7207(01)00656-6

Taruno, A., V. Vingtdeux, M. Ohmoto, Z. Ma, G. Dvoryanchikov, A. Li, L. Adrien, H. Zhao, S. Leung, M. Abernethy, et al. 2013. CALHM1 ion channel mediates purinergic neurotransmission of sweet, bitter and umami tastes. *Nature.* 495:223–226. http://dx.doi.org/10.1038/nature11906

VanGompel, M.J.W., and E.Y. Xu. 2011. The roles of the DAZ family in spermatogenesis: More than just translation? *Spermatogenesis.* 1:36–46. http://dx.doi.org/10.4161/spmg.1.1.14659

Veitinger, S., T. Veitinger, S. Cainarca, D. Fluegge, C.H. Engelhardt, S. Lohmer, H. Hatt, S. Corazza, J. Spehr, E.M. Neuhaus, and M. Spehr. 2011. Purinergic signalling mobilizes mitochondrial Ca^{2+} in mouse Sertoli cells. *J. Physiol.* 589:5033–5055. http://dx.doi.org/10.1113/jphysiol.2011.216309

Wu, L., M.R. Mashego, J.C. van Dam, A.M. Proell, J.L. Vinke, C. Ras, W.A. van Winden, W.M. van Gulik, and J.J. Heijnen. 2005. Quantitative analysis of the microbial metabolome by isotope dilution mass spectrometry using uniformly 13C-labeled cell extracts as internal standards. *Anal. Biochem.* 336:164–171. http://dx.doi.org/10.1016/j.ab.2004.09.001

Xiong, K., R.W. Peoples, J.P. Montgomery, Y. Chiang, R.R. Stewart, F.F. Weight, and C. Li. 1999. Differential modulation by copper and zinc of P2X2 and P2X4 receptor function. *J. Neurophysiol.* 81:2088–2094.

Yan, Z., S. Li, Z. Liang, M. Tomić, and S.S. Stojilkovic. 2008. The P2X7 receptor channel pore dilates under physiological ion conditions. *J. Gen. Physiol.* 132:563–573. http://dx.doi.org/10.1085/jgp.200810059

Yellen, G. 1984. Ionic permeation and blockade in Ca2+-activated K+ channels of bovine chromaffin cells. *J. Gen. Physiol.* 84:157–186. http://dx.doi.org/10.1085/jgp.84.2.157

Young, M.T., P. Pelegrin, and A. Surprenant. 2007. Amino acid residues in the $P2X_7$ receptor that mediate differential sensitivity to ATP and BzATP. *Mol. Pharmacol.* 71:92–100. http://dx.doi.org/10.1124/mol.106.030163

Zhang, Z., G. Chen, W. Zhou, A. Song, T. Xu, Q. Luo, W. Wang, X.S. Gu, and S. Duan. 2007. Regulated ATP release from astrocytes through lysosome exocytosis. *Nat. Cell Biol.* 9:945–953. http://dx.doi.org/10.1038/ncb1620